STATISTICAL DESCRIPTION OF A MAGNETIZED CORONA ABOVE A TURBULENT ACCRETION DISK

BY DMITRI A. UZDENSKY & JEREMY GOODMAN
Princeton University and
Peyton Hall, Princeton, NJ 08544
(Dated: March 3, 2008)
Draft version September 6, 2018

ABSTRACT

We present a physics-based statistical theory of a force-free magnetic field in the corona above a turbulent accretion disk. The field is represented by a statistical ensemble of loops tied to the disk. Each loop evolves under several physical processes: Keplerian shear, turbulent random walk of the disk footpoints, and reconnection with other loops. To build a statistical description, we introduce the distribution function of loops over their sizes and construct a kinetic equation that governs its evolution. This loop kinetic equation is formally analogous to Boltzmann's kinetic equation, with loop-loop reconnection described by a binary collision integral. A dimensionless parameter is introduced to scale the (unknown) overall rate of reconnection relative to Keplerian shear. After solving for the loop distribution function numerically, we calculate self-consistently the distribution of the mean magnetic pressure and dissipation rate with height, and the equilibrium shapes of loops of different sizes. We also compute the energy and torque associated with a given loop, as well as the total magnetic energy and torque in the corona. We explore the dependence of these quantities on the reconnection parameter and find that they can be greatly enhanced if reconnection between loops is suppressed.

Subject headings:

1. INTRODUCTION

Power-law components in the X-ray spectra of accreting black holes are attributed to hot, tenuous, quasi-spherical plasmas called *accretion disk coronae* (hereafter ADCe) by analogy with the solar corona, though comptonization rather than atomic lines or bremsstrahlung is thought to be the main emission mechanism in accreting systems (Bisnovatyi-Kogan & Blinnikov 1976; Liang & Price 1977). The vertical extent of ADCe is open to doubt since they are spatially unresolved and since the electron temperature inferred from high-energy spectral cutoffs, $T_e \sim 100\,\mathrm{keV}$, is typically small compared to the virial temperature of the ions, $T_i \sim 100\,\mathrm{MeV}$. Direct simulations of magnetorotational (hereafter MRI) turbulence in radiation-pressure-dominated disks show very large density contrasts and bulk velocities (Turner et al. 2002), so perhaps the power-laws are made within the disk itself (Socrates et al. 2004).

If a comptonizing corona indeed exists, then it is difficult to avoid the conclusion that it should be magnetically dominated. The electrons themselves cannot store much energy (Merloni & Fabian 2001): their Compton cooling time is at most comparable to the local dynamical time at luminosities $\gtrsim 10^{-2} L_{\mathrm{Edd}}$ and radii $\lesssim 20 GM_{\mathrm{bh}}/c^2$. Ions at virial temperatures would store much more energy but could not transfer it efficiently to the electrons by Coulomb collisions (Rees et al. 1982). Also, as in the solar case, magnetic fields are probably needed to convert mechanical energy of the optically thick regions into coronal heat. And since accretion is believed to be driven by MRI turbulence within the disk proper, it is expected that fields float up into the corona by Parker and interchange instabilities (Galeev et al. 1979; Tout & Pringle 1992).

Despite widespread recognition of these points, modelers of ADC emission rarely concern themselves with the dynamics of coronal magnetic fields. This is perceived to be too hard; certainly the long and arduous struggle to under-

stand the heating of solar corona—based on much more abundant data—tends to discourage hopes of solving the corresponding problem for accreting systems any time soon (*e.g.* Walsh & Ireland 2003; Klimchuk 2006). Attempts to model coronae through direct three-dimensional (3D) magnetohydrodynamic shearing-box (Miller & Stone 2000; Hirose et al. 2006) and global (Machida et al. 2000) simulations have been made, however. To date, such simulations suggest that while a magnetically dominated region does form, its vertical extent, when defined by distributions of shear stress or dissipation rate, exceeds that of the optically thick regions only modestly.

There are nevertheless good reasons to expect dynamically dominant coronae and to question the contrary evidence from simulations. On the one hand, a strongly magnetized corona may be required to extract power from black hole spin (Blandford & Znajek 1977) or from plunging gas inside the marginally stable orbit (Gammie 1999; Krolik 1999), or to drive a wind from the disk (Blandford & Payne 1982). A less widespread motivation, which however we feel strongly, is to reduce self-gravity in the outer parts of accretion disks in active galactic nuclei (at $r \gtrsim 10^3 GM_{\mathrm{bh}}/c^2$): a magnetized corona or wind might transport angular momentum more quickly than stresses limited to the optically thick layer, and thereby reduce the mass density within the disk for a given accretion rate (Goodman 2003).

On the other hand, codes designed for pressure-dominated plasmas may not be reliable when applied to magnetically dominated coronae. Shearing-box calculations cannot be trusted to represent magnetic structures much larger than a disk scale height (H) unless *all three* dimensions of the box are $\gg H$, which has not yet been achieved. Global simulations are unable to resolve thin disks and extended coronae unless the grid is made coarser in the corona than near the midplane, which increases numerical diffusion in the corona. This is not serious when $H \sim r$, as for the innermost parts of near-Eddington or radiatively inefficient accretion disks, where the X-ray evidence for coronae is strongest; but it would be a severe limitation for simulations of the marginally

self-gravitating parts of AGN disks, where $H/r \lesssim 10^{-2}$. These problems of spatial dynamic range will eventually be overcome with sufficient computer power.

A more fundamental difficulty for simulations has to do with magnetic reconnection. We will argue that the efficiency of reconnection[1] is crucial to the storage and dissipation of magnetic energy in ADCe, as it appears to be in the solar corona (Parker 1983, 1988; Klimchuk 2006). Reconnection in solar flares is observed to be "fast," meaning that annihilating field lines come together at a significant fraction of the local Alfvén speed. This is not well understood; because of the very high conductivity of the corona, MHD predicts reconnection rates slower by many orders of magnitude (Sweet 1958; Parker 1957). Collisionless plasma effects outside conventional resistive MHD may be necessary (Uzdensky 2007a,b, and references therein). Another mystery is what triggers fast reconnection, which does not always occur immediately but seems to require special conditions that have not been fully identified (Klimchuk 2006). The overall rate of magnetic dissipation depends both on the rate at which reconnection events are triggered and on the speed of reconnection during such events.

These complexities are elided by the astrophysical MHD codes used to study magnetorotational turbulence. Often in these codes, reconnection is purely numerical, that is, produced by truncation errors due to limited grid resolution. Explicit diffusivities are sometimes used, but if these are large enough make truncation errors unimportant, then they are necessarily orders of magnitude larger than astrophysical reality. Until recently, the general view among MRI simulators seems to have been that the microphysics of reconnection is unimportant. This view may be inspired by analogies with the dissipation of kinetic energy in hydrodynamic turbulence, both compressible and incompressible. Supersonic turbulence involves shocks, and as is well known, shock dissipation is independent of transport coefficients in the limit that these are small. On the other hand, three-dimensional incompressible turbulence involves inertial cascades such that dissipation, though occurring on small (viscous) scales, is entirely controlled by the dynamics on large scales and proceeds at rates that are again asymptotically independent of transport coefficients.

Whether or when turbulent *magnetic* dissipation is similarly independent of small—and therefore numerically unresolved—scales is an open question. Recent work indicates that magnetorotational turbulence is sensitive to the magnetic Prandtl number $P_m \equiv \nu/\eta$ (Lesur & Longaretti 2007; Fromang et al. 2007), at least in the range of fluid and magnetic Reynolds numbers ($Re \equiv VL/\nu$, $Re_m \equiv P_m Re$) accessible to direct simulations. It may be that Re_m and Re become unimportant when both are sufficiently large, but this has not yet been established even for kinematic dynamos, where the field is dynamically unimportant on all scales by construction (Boldyrev & Cattaneo 2004; Schekochihin et al. 2007, and references therein), much less for MRI turbulence. Even if this is true of systems in which fluid motions dominate the energy density, as they are presumed to do near the midplane of an accretion disk, the answer could be different for magnetically dominated systems such as ADCe. Perhaps relevant here is the case of turbulence in the presence of a dominant mean field, which has become somewhat better understood since the seminal paper of Goldreich & Sridhar (1995, hereafter GS95). Cascades do exist in such turbulence, with different scalings along and perpendicular to the mean field, so that the large scales are insulated from details at the resistive and viscous scales. However, there are at least two important differences between such systems and the nearly force-free ADCe contemplated in this paper. In the former systems, the Alfvénic propagation time along the field is assumed to be longer than the timescale of the cascade, so that the turbulent dynamics are local; by contrast, communication along the entire length of a line-tied coronal loop is effectively instantaneous compared to the timescale on which energy is injected into the loop by footpoint motions. The magnetic dynamics are therefore nonlocal, and not appropriately characterized as turbulent; a better description is a progression of force-free equilibria driven by changes at the boundary. [See, however, Rappazzo et al. (2007) for a contrary view.] Secondly, in GS95's Alfvénic cascades, the deviations from the mean field are small, and the cascade does not affect the energy in the large-scale mean field. In this paper, by contrast, we are concerned with coronal flux loops that reconnect with one another at large angles between their field lines. A significant fraction of the loops' magnetic energy may be liberated in such reconnection events, or in the relaxation to a new force-free equilibrium following topological changes brought about by reconnection.

It might be hoped that the MRI simulations could predict the total dissipation rate of the corona, if not its vertical distribution, because the rate of injection of energy to the corona is determined at its base, where thermal and kinetic energies dominate. This is a false hope, however. The rate of work done on the corona by the disk is proportional to the magnetic stress tensor at its base, specifically the rz and ϕz components of the stress. Insofar as the corona is approximately force-free, its total energy is expressible in terms of a boundary integral involving the same stress components. Thus if the coronal energy and magnetic configuration are incorrectly calculated, then the coronal dissipation rate is probably also incorrect. More concretely, because most of the kinetic energy available from the disk is the large-scale differential rotation rather than local turbulence, coronal field loops with large radial separations between their footpoints may be particularly important for the energy input; such loops are not possible in shearing-box simulations whose radial dimensions are no larger than the disk scale height, and even if the dimensions were increased, spurious reconnection might suppress the large loops. In short, for geometrical reasons and because they do not model reconnection correctly, present-day MRI simulations may underestimate the energies and dissipation rates of disk coronae.

The dynamics of ADCe may not be fully understood without great progress on all of the fronts described above: more powerful computations, better understanding of fast reconnection, and of course more incisive observations. Since all of this may take years or decades to accomplish, our purpose here is to try to imagine, in a disciplined way, some aspects of that ultimate understanding. Our approach is clearly indebted to Tout & Pringle (1996, henceforth TP96) but is richer in physical elements. We model the ADC as an assembly of closed magnetic loops with footpoints on the disk; open field is probably important but is deferred to a later paper because we do not wish to address winds here. We do not resolve

---

[1] It would be natural to write "rate of reconnection" here, but that this phrase is often used to mean the speed at which field lines of opposing polarities approach one another in a localized reconnection event, whereas we are concerned here with the global efficiency of reconnection in reducing magnetic energy.

the dynamics within the optically thick disk at all but treat the base of the corona as a dynamic boundary. It is assumed that the disk thickness is much less than its radius in the parts of the ADC that we model and that the loop lengths (L) lie at intermediate scales ($H \ll L \ll r$). Thus the lower boundary is conceived as an infinite plane. Small new loops are injected from this boundary, and existing loops are energized by the Keplerian shear if their footpoints lie at different radii. Loops reconnect in pairs according to prescribed rules with a frequency scaled relative to the shear by a dimensionless parameter. Each reconnection results in a new pair involving the same four footpoints differently connected, rather than a single loop as in TP96. The loop population is described by a distribution function over the length and orientation of the displacement from the negative to the positive-polarity footpoint (rather than the length alone as in TP96), and the processes of injection, stretching, and reconnection are incorporated in an integro-differential kinetic equation for the evolution of the loop distribution function.

Our model is not appropriate for all forms of ADCe. Following Liang & Price (1977), we presuppose a "sandwich" geometry in which the optically thick but geometrically thin disk coexists with its corona at the same radius. Such a geometry seems most appropriate to high/soft and very high states of galactic X-ray sources where the X-ray continuum shows both thermal and power-law features, and also to cases, both galactic and extragalactic, where a relativistically broad iron Kα line indicates that an optically thick disk, fluorescing under illumination by hard X-rays from the corona, extends down to the marginally stable orbit or beyond (*e.g.* Wilms et al. 2001; Miller et al. 2002). In low/hard states where only a power-law is seen, it may be that the inner parts of the thin disk have evaporated so that those regions are all "corona" (Esin et al. 1997); alternatively, the thin disk may persist down to the marginally stable orbit, but the corona may take the form of a mildly relativistic outflowing wind or jet, whose emission is directed away from the disk (Beloborodov 1999; Miller et al. 2006). The coronal model presented here would not apply to either of these cases without substantial modification.

In this paper, we explore what controls the magnetic energy, integrated stress, and dissipation rate of the corona; specifically, we explore the roles of shear and reconnection in this balance. Our overarching motivation is to determine under what conditions the corona contributes importantly to outward angular momentum transport: that is, to the torque that drives accretion through the disk. Secondary goals are to examine the distribution of energy, stress, and dissipation with height. We recognize that because of a number of questionable assumptions and simplifications, our model will hardly be the last word on this subject. We hope , however, at least to set up a target for future simulations to aim at, and to draw attention to certain quantities that could be extracted from existing simulations, such as the rate of emergence of flux dipoles (small loops) from the disk.

The outline of our paper is as follows. § 2 introduces our conception of magnetic loops and the loop distribution function. § 3 explores some properties of loops in equilibrium with the mean-field pressure exerted by neighboring loops: shape, maximum height, and energy. § 4 constructs the kinetic equation, including the rules for reconnection and other processes important to the evolution of the loop distribution. The numerical set-up used to solve the loop kinetic equation, including the boundary conditions at both small and large scales, is

described in § 5. In the same section we also present numerical solutions and discuss their implications for ADCe. In § 6 we discuss limitations of our model in the light of these results, and we indicate ways in which the model might be made more realistic. We attempt to relate what we have done to the present theoretical understanding of ADCe, and we discuss how simulations in the near future might be used to calibrate some features of our model, for example the rate of emergence of small loops from the disk. Finally, § 7 summarizes our main conclusions.

2. STATISTICAL DESCRIPTION OF THE ADC MAGNETIC FIELD

As noted in §1, there are fundamental physical similarities between the formation processes of the solar and accretion disk coronae. At the same time, one has to keep in mind the important differences between them. These include: (1) differences in the underlying sub-photospheric turbulence (thermal convection vs. MRI); (2) a strong large-scale differential rotation and shear in disks, whereas small scales dominate the shear in the Sun; (3) the possibility of strong magnetocentrifugally- and radiation-driven winds from an accretion disk, as compared to the relatively weak thermally driven solar wind; (4) Compton cooling of the disk corona in black hole systems; (5) a greater separation of spatial scales in thin disks between the disk thickness and its radius, as opposed to the solar case, where the convection zone spans a significant fraction of the Sun's radius, which results in the generation and emergence of very large magnetic structures associated with sunspots in active regions. Finally, we have only one Sun, whereas there is a large variety of astrophysical accretion-disk systems, some of which have coronae.

In addition to the above, there is an important basic difference in our observational capabilities: whereas the Sun is so close that we can spatially resolve *individual* events and structures in the solar corona (such as flares, loops, etc), such resolution is not available for ADCe. Therefore, we can study only the spatially-integrated spectral and timing properties of the disk corona. This fact provides a strong motivation for focusing on a *statistical description* for the magnetic field in the ADC.

Here is, briefly, the basic physical picture of the magnetized corona above a turbulent accretion disk. The corona is a dynamic, self-organized system that can be represented by a statistical ensemble of flux loops (Tout & Pringle 1996; Hughes et al. 2003). The loops continuously emerge out of (and submerge into) the disk as a result of magnetic buoyancy. Once above the surface, they constantly evolve due to a number of physical processes. They are twisted and stretched by the differential keplerian rotation and by the random motions of their footpoints on the disk's surface, which causes the individual loops to inflate. As a result, the magnetic field in the corona becomes non-potential and highly stressed; an appreciable amount of free magnetic energy can thus be stored in the corona. However, in the process of twisting and expansion the loops may undergo internal disruptions due to MHD instabilities and also may reconnect with other loops. Such relaxation events manifest themselves as flares; they bring the field closer to the potential state and thus enable the inflation process to resume. At the same time, reconnection between loops sometimes produces more spatially-extended magnetic structures in the corona (the coronal "inverse cascade"). Finally, all these complicated processes occur repeatedly over and over, simultaneously on various spatial scales. Thus, the corona can be viewed as a *boiling magnetic foam*,
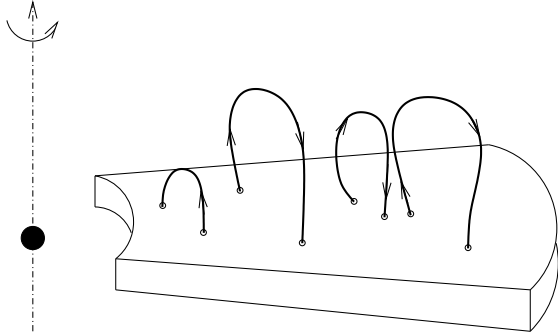
FIG. 1.— Schematic view of ADC as an ensemble of many magnetic loops.

FIG. 2.— Closed magnetic loop as the main structural element of a magnetized accretion disk corona.

in which magnetic loops repeatedly swell and grow because of the magnetic energy pumped into them by the footpoint motions and then snap and contract back due to reconnective disruptions and sometimes merge to form bigger structures.

What is the appropriate statistical language for describing a chaotic, highly intermittent magnetized corona above a turbulent accretion disk? At a most general level, we describe the corona by an ensemble of some *elementary magnetic structures*. Each of these fundamental individual constituents of the corona is characterized by a small set of primary physical parameters. The individual elements evolve with time according to certain rules that reflect the relevant physical processes that we believe are most important in shaping the corona. These processes generally include various forms of interaction between elements. Mathematically, the evolution rules are represented by stochastic (Langevin) equations of motion of magnetic elements in the primary parameter space. Since we are interested in a statistical description, we introduce a distribution function of our magnetic elements in the primary-parameter phase-space. Correspondingly, one of our main goals is to derive the equation for the evolution of this distribution function, using the equations of motion of individual elements. This is done by analogy with the way the Boltzmann kinetic equation for the particle distribution function in a gas is derived in Statistical Mechanics, but obviously is more *ad hoc* in our case. Finally, there are several important integral quantities in our theoretical framework, which are related to moments of the distribution function. These self-consistent quantities represent the mean-field interaction between the magnetic elements and they affect the evolution of the distribution function.

2.1. *The Loop Distribution Function*

Based on the above discussion, we shall now build a calculable model of the corona. Our first task is to select the most appropriate and most fundamental elementary magnetic constituents of the corona. We shall then need to select the most natural set of parameters describing these elements.

Guided by the analogy with the solar corona, we shall use simple (anchored in the disk at both ends, see Fig. 2) magnetic loops, or flux tubes, as our fundamental magnetic elements — the main structural constituents of the corona. This choice is influenced by the existing theoretical work in both solar physics (*e.g.* Hughes et al. 2003), and also in ADC (Tout & Pringle 1996). Such loops represent the closed magnetic field corresponding to zero net vertical flux through the disk. This is a natural assumption for the case when the magnetic field in the corona comes from the flux emergence of the
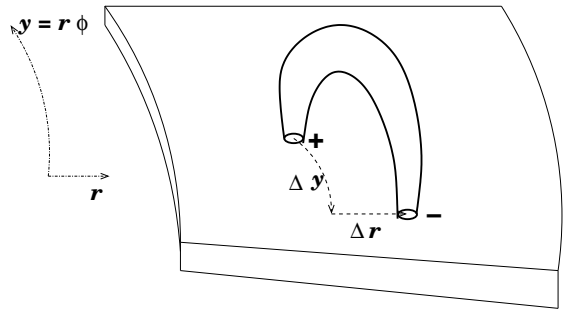
field generated by the dynamo in the disk itself. In this paper we shall assume that this is indeed the case. In principle, however, one may also wish to consider a more general situation where, in addition to the closed coronal loops, there is also an external large-scale open magnetic field through the disk, such as may be coming from the central star or the interstellar medium (see § 6.1).

For simplicity, we shall characterize each loop by only two primary parameters: *(i)* the radial footpoint separation $\Delta r = r_- - r_+$, and *(ii)* the azimuthal footpoint separation $r\Delta\phi = \Delta y = y_- - y_+$ (see Fig. 2). Thus, we shall measure Δr and Δy from the "+" magnetic footpoint to the "-" magnetic footpoint. This means that Δr and Δy can be positive or negative depending on the orientation of the loop. Alternatively, sometimes we will use an equivalent representation in terms of the loop's projected length (the distance between the loop's footpoints): $L \equiv (\Delta r^2 + \Delta y^2)^{1/2}$; and the orientation angle, θ, measured clockwise with respect to the toroidal direction: $\theta \equiv \arctan(\Delta r/\Delta y)$.

In a more general description, one may enlarge the parameter space to include additional parameters, such as the magnetic flux $\Delta\Psi$ contained within a loop, or the loop's twist (see § 6.2). However, since our goal here is to build the simplest version of this already very complicated theory, we shall assume that all the loops have the same magnetic flux $\Delta\Psi$ and, furthermore, that they are not twisted. The latter assumption means that the magnetic field within each loop is purely potential, *i.e.*, that the bulk of the corona is nearly current-free and all the coronal currents flow along inter-loop boundaries.

In addition to the above two primary parameters, we shall also need some secondary parameters describing a given loop, such as the loop's overall shape, its maximum height Z_{top} above the disk; and its thickness at a given height, $d(z)$. These quantities will be useful for estimating the loop expansion rate and for analyzing binary interaction (reconnection) of loops with each other. In our model, these secondary parameters are uniquely determined by the primary ones in combination with the self-consistent mean field $\bar{B}(z)$ (see § 3.2).

Note that a loop carrying a finite flux $\Delta\Psi$ has a certain finite thickness (in the radial and azimuthal directions) at the disk surface. For a typical loop, this thickness is generally of order H. Therefore, instead of a pair of footpoints that a field *line* would have, a finite-thickness *loop* has a pair of footspots. Thus, we need to be a little bit more precise in our definitions of Δr and Δy. We shall define them as the radial and azimuthal separations between the centers of the two footspots, that is between the two footpoints of the central field line of the loop (magnetic axis for a twisted loop).

Following Tout & Pringle (1996), we introduce the *loop distribution function*, $F(\Delta r, \Delta y)$, defined so that $F(\Delta r, \Delta y)d\Delta rd\Delta y$ is the number of loops with the values of primary parameters in the range ($[\Delta r, \Delta r + d\Delta r], [\Delta y, \Delta y + d\Delta y]$), per unit disk area. Alternatively, we may write the distribution function in terms of loop length $L = (\Delta r^2 + \Delta y^2)^{1/2}$ and orientation $\theta = \arctan(\Delta r/\Delta y)$, *i.e.*, $F(L, \theta)$. The overall normalization of the distribution function is determined by the requirement that loops cover the entire disk surface; it will be discussed in more detail in § 3.2.

2.2. *Role of Magnetic Reconnection in ADCe*

At the most basic level, the corona (either solar or ADC) is perfectly conducting almost everywhere. However, as it evolves driven by the complex turbulent motions of the magnetic footpoints on the surface, the corona may develop numerous current sheets on a variety of scales (Parker 1972, 1983). These current sheets are possible sites of dissipation of magnetic energy *via* reconnection. In fact, reconnection is one of the most essential nontrivial physical processes that govern the complex dynamical behavior of the corona. In particular, it controls the vertical extent of the corona (*e.g.*, the coronal magnetic scale-height H_B). Indeed, if reconnection were too efficient, then the coronal field would be nearly potential and $H_B \sim H$; then, the free magnetic energy stored in the corona would be small, as would the magnetic dissipation rate.

On the other hand, if no reconnection were allowed at all, then, magnetic loops would, over time, grow bigger and bigger in height because of the differential Keplerian rotation. Unable to dissipate, magnetic energy would continuously accumulate in the corona as the characteristic magnetic scale-height H_B increases, essentially linearly in time. This phase would continue until H_B becomes comparable to the disk radius, $H_B \sim r \gg H$. After that, radial gradients become important and the subsequent evolution would enter a qualitatively different regime characterized by accelerated expansion of the magnetic loops, which effectively would become open, perhaps even in a finite time (van Ballegooijen 1994; Lynden-Bell & Boily 1994; Aly 1995; Sturrock et al. 1995; Uzdensky 2002). The corona would then consist of a dense forest of open flux tubes of alternating polarity separated by a multitude of current sheets. Unless there are significant mass-loaded winds (violating the force-free assumption), the power pumped into the corona would then go down, and the accumulated free magnetic energy would saturate at a value corresponding to a fully open (split-monopole) magnetic field (Aly 1991; Sturrock 1991). Although this asymptotic energy would be very large, of order r/H larger than that of the fully closed potential field, it would still remain finite; this is because the toroidal magnetic field at the disk surface and hence the work done on the coronal magnetic field by the Keplerian disk shear would both go to zero. Similarly, the angular momentum exchange between different parts of the disk due to coronal loops would also go down. As new flux tubes emerged from the disk, the magnetic forest would become ever more dense. The corona would thus look very different from what we expect. We thus see that reconnection is necessary for maintaining a *meaningful* statistical steady state. It enables open field lines to close back and thus restores the magnetic connection between different parts of the disk. This, in turn, facilitates angular-momentum transport *via* the coronal magnetic field [coronal MRI, (Goodman 2003); see also (Heyvaerts & Priest 1989; Pavlidou et al. 2001)]. Strong

magnetic dissipation and large torque thus require some intermediate reconnection efficiency, neither so rapid as to keep the field nearly potential, nor so slow as to allow it to become fully open; in both limits, the torque and energy dissipation rate vanish.

Another reason why reconnection is important is that a growing magnetic loop may reconnect with another one connected to a very different place on the disk. This process may lead to an *"inverse cascade"* of magnetic loops (Tout & Pringle 1996). It is an important avenue towards building up a population of loops with large radial footpoint separation. Indeed, whereas Keplerian differential rotation increases the azimuthal footpoint separation of a loop, it does not affect its radial footpoint separation. Therefore, without reconnection, the radial footpoint separation of a coronal flux loop would change only relatively slowly by the random walk of its footpoints due to the underlying disk turbulence. In principle, the footpoints will drift radially apart in direct response to the angular momentum transfer by the coronal loop itself (we call this process "coronal MRI"). The characteristic velocity of this drift is on the order of $B^2/4\pi\Sigma\Omega$, where Σ is the surface density of the disk. The resulting relative increase in Δr on the rotation-period timescale is of the order of $\delta\Delta r/\Delta r \sim B^2/4\pi\Sigma\Delta r\Omega^2$. Using $\Sigma \simeq H\rho$ and $H \sim c_s/\Omega$, where c_s and ρ are the sound speed and the gas density within the disk, we can estimate that $\delta\Delta r/\Delta r \sim (V_A/c_s)^2 H/\Delta r \equiv \beta^{-1}H/\Delta r$, where $V_A^2 \equiv B^2/4\pi\rho$ is the Alfvén speed within the disk. Thus, since we are mostly interested in large loops, $\Delta r \gg H$, we see that Δr cannot grow appreciably without reconnection. *Thus reconnection is necessary for the coronal "inverse cascade".*

In addition, magnetic reconnection in the corona regulates the fraction of the magnetic flux that is open at any given time and also the effective radial transport of a large-scale vertical magnetic field Spruit & Uzdensky (2005); Fisk (2005). Both of these processes are important for establishing large-scale disk outflows.

Finally, as in the solar corona, reconnection is believed to be the main mechanism of releasing the accumulated magnetic energy, leading to coronal heating and observed high-energy coronal emission.

3. THE SELF-CONSISTENT CORONA

In principle, the loop distribution function $F(L, \theta)$ contains enough information to fully describe the statistical magnetic structure of the corona. This means that, once $F(L, \theta)$ is known, one should be able to answer most of the questions posed in §1. In particular, one should be able to derive the actual shapes and heights, $Z_{top}(L)$, of coronal loops, the distribution of magnetic energy with height, $\bar{B}^2(z)/8\pi$, the energy $\mathcal{E}(L)$ associated with a loop of a given size, the torque transmitted by the coronal magnetic field, etc. In this section we demonstrate how to do all this.

3.1. *Equilibrium Shape of a Loop in a Stratified Atmosphere*

First, we shall work out the correct shape of an isolated slender (with a cross-sectional diameter $d \ll L$) untwisted loop $\mathcal{A}$ carrying magnetic flux $\Delta\Psi$, immersed in a medium with some isotropic but, in general, nonuniform pressure $P(z)$ (see Fig. 3). This pressure represents the confining magnetic pressure of all other loops; thus, for actual calculations, it will be convenient to write $P(z)$ as $P(z) \equiv \bar{B}^2(z)/8\pi$. The shape of the loop is then determined by the requirement that the loop be in magnetostatic equilibrium with this external pressure.
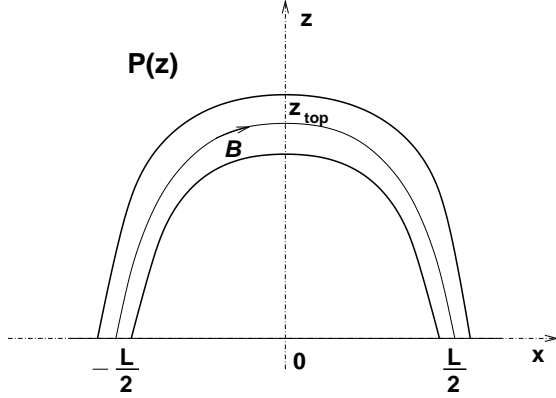
FIG. 3.— Untwisted isolated loop confined by external isotropic pressure $P(z)$.

FIG. 4.— Infinitesimal loop segment.

First, the local pressure balance across the loop gives us the magnetic field strength inside it as a function of height:

$$B(z) = \sqrt{8\pi P(z)} \equiv \bar{B}(z). \qquad (1)$$

Then, since the magnetic flux is constant along the loop, we can write the local cross-sectional area $a(z)$ of the loop in terms of $\bar{B}(z)$:

$$a(z) = \frac{\Delta\Psi}{\bar{B}(z)}. \qquad (2)$$

Now let us discuss equilibrium shape $x(z)$ of a slender loop as a whole, represented by the shape of the loop's central field line. First, we would like to note that, for a curved but untwisted loop confined by a *uniform* external pressure P_0, it is impossible to find an equilibrium shape. Indeed, since the field inside the loop has no twist and is purely axial (*i.e.*, runs along the loop), it is a potential field produced by perpendicular (to the direction of the loop) currents flowing on the loop's surface. Therefore, at any given location along the loop, the magnetic field strength is slightly nonuniform in the cross-loop direction: it drops off as $1/R$, where R is the local curvature radius ("major radius" in tokamak terminology). In other words, the magnetic force balance between the magnetic pressure and the magnetic tension inside a curved loop means that there must be a magnetic pressure gradient to balance the tension force due to the curvature. Therefore, the magnetic field on the underside (the "inboard", in tokamak terminology) of the loop is larger than that on the upside (the "outboard"). On the other hand, however, the magnetic field at each point on the surface of the loop has to be in pressure balance with the external pressure $P(z)$. If $P(z) = P_0 = $ const, this pressure balance means that the magnetic field has to be uniform along the loop's boundary. Thus, we have a clear incompatibility between the assumption that the loop is curved but untwisted and the condition of local force balance with an external uniform pressure.

This phenomenon can also be understood using the notion of Pfirsch–Schlüter currents, a well-known concept in tokamak physics. Since the magnetic field inside an untwisted flux tube is strictly in the axial direction (along the tube), the currents that produce it flow on the skin of the tube in the perpendicular direction. But since the currents have to close, and since the tube is curved, the surface current density (*i.e.*, the current per unit length along the tube) is bigger on the underside than on the upside. Then, according to Ampere's law, the magnetic field is also stronger on the underside, and
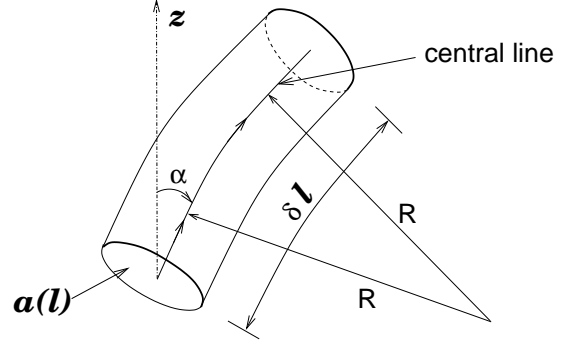
thus cannot be in pressure equilibrium with a uniform external pressure on both sides simultaneously. The only way a curved loop can be in equilibrium with uniform external pressure, is when the surface current density is also uniform. Since the current has to be conserved, this requires that some surface current should also flow along the loop (the so-called Pfirsch–Schlüter current), and hence the magnetic field must be twisted.

These considerations show that an untwisted flux tube confined by a uniform external pressure has to be straight. If, however, the pressure is not uniform, then an equilibrium shape for a curved tube can be found, as we now show.

Let us consider a case with pressure $P(z)$ decreasing monotonically with height. Consider a slender loop in the (x, z) plane, symmetric with respect to $x = 0$, with its two footpoints at $x = \pm L/2$ (see Fig. 3). The shape of the loop as a whole, described by a symmetric function $z(x)$, is determined by the perpendicular (to the magnetic field) force-balance between tension and the pressure-gradient forces. The force-balance is established at every point along the loop. To analyze it at a given location on the loop, let us consider a small loop segment. We shall denote the arc-length along the loop, measured from its left footpoint, by l. For clarity of discussion, let us represent the loop segment locally by a slightly curved cylinder of length $\delta l \ll L$, cross-sectional area $a(l)$, and curvature radius $R(l)$ (see Fig. 4). Let us also introduce the angle $\alpha(l)$ between the magnetic field and the vertical direction:

$$\cos\alpha = \frac{dz}{dl}. \qquad (3)$$

For definiteness, we consider the ascending leg of the loop, where $B_z > 0$, so that $0 \le \alpha \le \pi/2$. The local curvature radius $R(l)$ of the loop is related to $\alpha(l)$ *via*

$$\frac{1}{R} = \frac{d\alpha}{dl}. \qquad (4)$$

Here we treat $\bar{B}(z)$ as a known function and our goal is to determine the geometrical shape of the loop described by $\alpha(z)$.

The magnetic tension force on the loop segment acts in the direction of its curvature radius $\hat{R}$ and is equal to

$$\delta f_{\text{tension}} = \frac{B^2}{4\pi R}\, a(l)\, \delta l, \qquad (5)$$

The projection of the external-pressure force on the loop segment onto $\hat{R}$ can be written as

$$\delta f_{\nabla P} = -\frac{dP}{dz}\, \sin\alpha\, a(l)\, \delta l. \qquad (6)$$

Then, the force-balance condition can be written simply as

$$\frac{B^2}{4\pi}\frac{1}{R} = -\sin\alpha\,\frac{dP}{dz}, \qquad (7)$$

or, making use of equation (1),

$$\frac{\bar{B}(z)}{R} = -\sin\alpha\,\frac{d\bar{B}}{dz}. \qquad (8)$$

Combining this equation with the geometrical relation (4), we immediately obtain:

$$\frac{d\alpha}{dl} = \frac{1}{R} = -\frac{d\log\bar{B}}{dz}\sin\alpha. \qquad (9)$$

[Note that, as one can immediately see, a magnetic loop can be in equilibrium with a uniform $[\bar{B}(z) = \text{const}]$ external pressure only if it is straight, $\alpha = \text{const}$.]

Using (3), we get

$$\cot\alpha\,\frac{d\alpha}{dz} = -\frac{d\log\bar{B}}{dz} \quad\Rightarrow\quad \sin\alpha(z) = \frac{C}{\bar{B}(z)}. \qquad (10)$$

It is interesting to note that the same result can be obtained in a simple and elegant way by using a variational principle, namely, by by minimizing the loop's magnetic energy $E_{\text{magn}} = (\Delta\Psi/8\pi)\int B(l)\,dl$ (see § 3.4) viewed as a functional of $z(x)$. Using the relationship $dl = dx\,\sin^{-1}\alpha$, we have

$$\delta E_{\text{magn}}[z(x)] = \frac{\Delta\Psi}{8\pi}\,\delta\int B[z(x)]\sqrt{1+z'^2(x)}\,dx$$
$$= \frac{\Delta\Psi}{8\pi}\int\left[B'(z) - B(z)\frac{z''}{1+z'^2}\right]\frac{\delta z(x)\,dx}{\sqrt{1+z'^2}}. \qquad (11)$$

From the condition $\delta E_{\text{magn}} = 0$, we thus immediately get

$$B = C\sqrt{1+z'^2(x)} = C\frac{dl}{dx} = \frac{C}{\sin\alpha}, \qquad (12)$$

which, taking into account that $B = \bar{B}(z)$, is the same as the above result (10).

The result (10) means that the horizontal (x) component of the magnetic field is constant along the loop:

$$B_x(l) = B\sin\alpha = \bar{B}(z)\sin\alpha = C = \text{const}. \qquad (13)$$

The integration constant C is just equal to the magnetic field B_{top} at the top of the loop (where $\alpha = \pi/2$). Thus, the shape of the loop is given by the equation

$$\sin\alpha(z) = \frac{B_{\text{top}}}{\bar{B}(z)}. \qquad (14)$$

We can now work out an explicit expression for the field line shape $z(x)$ in terms of the function $b(z) \equiv \bar{B}(z)/\bar{B}(z=0)$. Let us denote the magnetic field strength at the base by $B_0 \equiv \bar{B}(z=0)$ and the angle between the loop and the vertical direction at the base by $\alpha_0(L) = \alpha(z=0;L)$. We then have

$$b_{\text{top}}(L) = \frac{\bar{B}_{\text{top}}(L)}{B_0} = \sin\alpha_0(L). \qquad (15)$$

Then, the shape of the ascending leg of a loop of length L is given by

$$x(z) = -b_{\text{top}}\int_z^{z_{\text{top}}}\frac{dz'}{\sqrt{b^2(z')-b_{\text{top}}^2}} = -\frac{L}{2} + b_{\text{top}}\int_0^z\frac{dz'}{\sqrt{b^2(z')-b_{\text{top}}^2}}. \qquad (16)$$

The height of the loop, z_{top}, is determined implicitly by the condition $x(z_{\text{top}}) = 0$:

$$\frac{L}{2} = b_{\text{top}}\int_0^{z_{\text{top}}}\frac{dz'}{\sqrt{b^2(z')-b_{\text{top}}^2}}. \qquad (17)$$

Analogous expressions have been obtained by Parker (1975) and Browning & Priest (1984).

Here are a few analytical examples of the use of this relationship.

1) Example I:

$$b(z) = \frac{1}{1+\zeta}, \qquad (18)$$

where $\zeta = z/z_0$; z_0 represents the characteristic magnetic scale height of the corona. Then we get $b_{\text{top}}(L) = 2z_0(4z_0^2+L^2)^{-1/2}$, and $z_{\text{top}}(L) = (z_0^2+L^2/4)^{1/2} - z_0$.

2) Example II: exponential atmosphere,

$$b(z) = e^{-z/H} \qquad (19)$$

Performing the integration (17), we obtain $x(z) = -H\arctan[e^{2(z_{\text{top}}-z)/H}-1]^{1/2}$, and correspondingly,

$$L(Z_{\text{top}}) = 2H\arccos[b(Z_{\text{top}})] = 2H\left[\frac{\pi}{2}-\alpha_0(Z_{\text{top}})\right]. \qquad (20)$$

Notice that for tall loops with $Z_{\text{top}} \gg H$ and $b_{\text{top}} \ll 1$, the dependence $L(Z_{\text{top}})$ saturates: $L(Z_{\text{top}}) \to L_{\text{max}} = \pi H$. This example illustrates an important point: if the external pressure drops off sufficiently steeply, then there is a maximum projected length, L_{max}, that a loop in equilibrium can have. This implies that if one tries to insert a slender loop with a foot-point separation $L > L_{\text{max}}$, then such a loop will not be able to attain an equilibrium and will instead grow in height without bound, *i.e.*, will tend to open up.

This fact points to an important feedback: for a given external pressure profile, large loops extend to larger heights, but this has an effect of increasing the contribution of these loops to the pressure at these large heights (see below), and hence may make the pressure profile less steep.

3.2. Magnetic Energy Density $\bar{B}^2(z)/8\pi$ as a Self-Consistent Mean Field

Our next step is to determine $\bar{B}$ as a function of z. However, the best way to do this is first to express $\bar{B}$ directly in terms of the length of the smallest loop L that reaches the given height z, *i.e.*, to find $\bar{B}(L)$. This can be done directly in terms of the orientation-integrated distribution function $\bar{F}(L) \equiv \int F(L,\theta)d\theta$, since, at any given height z, contributions to the magnetic pressure $\bar{B}^2/8\pi$ come only from those loops that extend to this height or higher. Since the dependence $Z_{\text{top}}(L)$ is presumed to be monotonic, then $\bar{B}$ at a given height z will be proportional, roughly speaking, to the integral over all loops with lengths $L > L(z)$, where $L(z)$ is the function inverse to $Z_{\text{top}}(L)$. Thus, naively, we anticipate a result that looks something like this:

$$\bar{B}(L) \sim \Delta\Psi\int_L^\infty\bar{F}(L)\,dL. \qquad (21)$$

In Appendix A we perform a rigorous analysis and derive an exact (within our model) result:

$$db = -\frac{\pi\,\Delta\Psi}{B_0}\,\bar{F}(L)\,dL \quad\Rightarrow\quad b(L) = \frac{\pi\,\Delta\Psi}{B_0}\int_L^\infty\bar{F}(L')\,dL', \qquad (22)$$

that is,

$$B_{\text{top}}(L) = \pi \Delta\Psi \int\limits_{L}^{\infty} \bar{F}(L')\,dL'. \tag{23}$$

The condition $b(z=0) = 1$, in conjunction with $Z_{\text{top}}(L=0) = 0$, gives us the normalization condition for the function $\bar{F}(L)$:

$$\int\limits_{0}^{\infty} \bar{F}(L')\,dL' = \frac{B_0}{\pi \Delta\Psi}. \tag{24}$$

If all the loops were perpendicular to the disk surface, the normalization coefficient would be 1/2 (since each loop has two footpoints). The extra factor $(2/\pi)$ in the above expression reflects the fact that small low-lying loops are not perpendicular to the disk surface, and hence occupy larger horizontal projected area on this surface.

For a given loop distribution function $\bar{F}(L)$, one can thus compute, in principle, the function $b(L)$ that we shall need in the next subsection.

3.3. *Self-Consistent Loop Height* $Z_{\text{top}}(L)$

Once $L(b_{\text{top}})$ is thus determined, we can substitute it into equation (17) and thus reduce the whole problem to the following integral equation for the function $U(b) \equiv dz/db$:

$$\frac{L(b)}{2b} = -\int\limits_{b}^{1} \frac{U(b')\,db'}{\sqrt{b'^2 - b^2}}. \tag{25}$$

Once this equation is solved, we can integrate $U(b)$ to find $z(b)$, thus completing the solution.

Mathematically, equation (25) is a linear Volterra integral equation of the first kind for the function $U(b)$ in terms of a known function $L(b)$. It can be solved exactly. In particular, by a simple transformation of variables: $t \equiv 1 - b'^2$, $s \equiv 1 - b^2$, $G(s) \equiv L(b)/2b$, and $V(t) \equiv -U(b')/2b'$, it can be transformed into the Abel equation:

$$\int\limits_{0}^{s} \frac{V(t)\,dt}{\sqrt{s-t}} = G(s). \tag{26}$$

whose solution is

$$V(s) = \frac{1}{\pi} \frac{d}{ds} \int\limits_{0}^{s} \frac{G(t)\,dt}{\sqrt{s-t}} = \frac{1}{\pi} \int\limits_{0}^{s} \frac{G'(t)\,dt}{\sqrt{s-t}}, \tag{27}$$

where we have used $G(s=0) = L(z=0)/2 = 0$.

Actually, the most useful form of the solution is the first equality in equation (27). By substituting the definitions of $V(s)$, $G(s)$ and $U(b)$ into this equation, multiplying by $(-2b)$ and integrating with respect to b, we get the following elegant final expression for the function $z(b)$:

$$z(b) = \frac{1}{\pi} \int\limits_{b}^{1} \frac{L(b')\,db'}{\sqrt{b'^2 - b^2}}. \tag{28}$$

Using equation (23), we can rewrite this in terms of the functions $\bar{F}(L)$ and $b(L)$ as

$$Z_{\text{top}}(L) = \frac{\Delta\Psi}{B_0} \int\limits_{0}^{L} \frac{L'\,\bar{F}(L')\,dL'}{\sqrt{b^2(L') - b^2(L)}}. \tag{29}$$

3.4. *Loop Energy*

One of the main goals of this section is to address the *energetics* of the magnetized corona. Relevant issues include the energy distribution of flares as well as the torque on the disk due to the coronal magnetic fields. In order to be able to address this, we must first determine the energy, $\mathcal{E}(\mathcal{A})$, associated with a loop of type $\mathcal{A}$.

The loop energy is given by the work done by the footpoints against magnetic forces as the loop's footpoint separation (*i.e.*, the projected length of the loop) is increased from zero to its present value L. Since we regard $P(z)$ as isotropic, the energy depends only on the length but not on the orientation of the loop:

$$\mathcal{E}(\mathcal{A}) = \mathcal{E}(L) = \int\limits_{0}^{L} f_{\text{fp}}(L')\,dL'. \tag{30}$$

Here, $f_{\text{fp}}(L)$ is the magnetic force on each of the two footpoints; it is proportional to the horizontal magnetic field $B_{\text{hor}}(z=0)$ at the disk surface:

$$f_{\text{fp}}(L) = \left.\frac{B_z B_{\text{hor}}}{4\pi}\right|_{z=0} a_{\text{hor}}(z=0) = \frac{\Delta\Psi}{4\pi} B_{\text{hor}}(z=0;L), \tag{31}$$

where $\Delta\Psi$ is the magnetic flux carried by the loop and $a_{\text{hor}}(z=0) = \Delta\Psi/B_z(z=0)$ is the area of the loop's footspot on the disk surface.[2] Thus, we have

$$\mathcal{E}(L) = \frac{\Delta\Psi}{4\pi} \int\limits_{0}^{L} B_{\text{hor}}(z=0;L')\,dL'. \tag{32}$$

Another quantity of interest is the magnetic energy E_{magn} contained within the loop:

$$E_{\text{magn}} = \int a(l) \frac{B^2(l)}{8\pi}\,dl, \tag{33}$$

where the integral is taken along the loop from one footspot to the other. Using flux conservation, $\Delta\Psi(l) = a(l)B(l) = \text{const}$, this energy can be written simply as

$$E_{\text{magn}} = \frac{\Delta\Psi}{8\pi} \int B(l)\,dl. \tag{34}$$

This expression actually has a very simple physical meaning. The integral $\int B(l)\,dl$ is the circulation of the magnetic field along the loop; according to the Ampere's law, this is just the total surface current flowing around the loop in the perpendicular direction. Thus, the above expression for E_{magn} is just a manifestation of the well-known result that the magnetic energy of a current circuit is proportional to the product of the magnetic flux enclosed by the circuit and its total current.

We would like to remark that $\mathcal{E}(L)$ can be viewed as a magnetic enthalpy, H_{magn}. It includes both the magnetic energy E_{magn} stored within the loop and the work W done by the loop on the surrounding gas with a fixed (but not necessarily uniform) pressure profile:

$$d\mathcal{E} = dH_{\text{magn}} = dE_{\text{magn}} + dW. \tag{35}$$

This is analogous to calculating the amount of heat Q required to inflate a hot-air balloon at constant atmospheric pressure P_0. Indeed, when the balloon air is heated, the energy is expended both to increase the internal energy U of

---

[2] Note that here, instead of fixing $\Delta\Psi$ and $B_z(z=0)$, we fix $\Delta\Psi$ and the total magnetic field $B(z=0)$, which includes the horizontal component.

the hot air inside the balloon and to perform work against atmospheric pressure (neglecting heat losses from the balloon through its skin). Thus, the amount of heat that needs to be supplied is equal to the change in balloon's enthalpy H:

$$dQ = dH = dU + P_0 dV = \frac{1}{\gamma - 1} d(P_0 V) + P_0 dV = \frac{\gamma}{\gamma - 1} P_0 dV ,$$
(36)

where γ is the adiabatic index of air. In our case of a magnetic loop confined by external pressure, the adiabatic index is $\gamma = 2$. Therefore, we expect that the total energy that needs to be supplied by the footpoint motions to inflate the loop is twice the internal magnetic field energy within the loop:

$$\mathcal{E} = E_{\mathrm{magn}} + W = 2 E_{\mathrm{magn}} .$$
(37)

In Appendix B we demonstrate that this is indeed so.

Note that, in addition to the work W done against the external gas pressure as the loop expands and increases its cross-section, there is also the work done against the magnetic tension force as the length of the loop is increased and the work done on the loop by the external pressure-gradient force. However, as long as the loop expands quasi-statically, always maintaining its equilibrium shape, the last two forces precisely balance each other (see § 3.1), and so their corresponding works cancel out.

Using the formalism developed in the previous subsections, we can now easily calculate the energy associated with a given loop. Substituting equation (13) into equation (32) and using expression (23) for $B_{\mathrm{top}}(L')$, we get

$$\mathcal{E}(L) = \frac{\Delta\Psi}{4\pi} \int_0^L B_{\mathrm{top}}(L')\, dL' = \frac{\Delta\Psi^2}{4} \int_0^L \int_{L'}^\infty \bar{F}(L'')\, dL''\, dL' .$$
(38)

The total magnetic energy in the corona is then

$$E_{\mathrm{tot}} = \frac{1}{2} \int_0^\infty \bar{F}(L)\,\mathcal{E}(L)\, dL = \frac{\Delta\Psi^2}{8} \int_0^\infty dL \int_0^L dL' \int_{L'}^\infty dL''\, \bar{F}(L)\,\bar{F}(L'')$$

$$= \frac{\Delta\Psi^2}{4} \int_0^\infty dL \int_0^L dL'\, L'\, \bar{F}(L)\,\bar{F}(L') .$$
(39)

It is instructive to consider a case in which $\bar{F}(L)$ has a power law tail, $\bar{F} \sim L^{-\alpha}$, truncated at some large $L_{\max} \gg H$. Then, as can be seen from equation (38), the energy of the largest loop, $\mathcal{E}(L_{\max})$, is almost independent of $L_{\max}$ for $\alpha > 2$, but starts to grow as $L_{\max}^{2-\alpha}$ for $\alpha < 2$. In a similar manner, from equation (39) it follows that the total coronal energy becomes dominated by the large-L tail if $\bar{F}(L)$ drops off sufficiently slowly, i.e., $\alpha < 3/2$. In this case the total energy scales with $L_{\max}$ as $E_{\mathrm{tot}} \propto L_{\max}^{3-2\alpha}$ and may become much larger than the potential magnetic field (whose characteristic magnetic scale height is of order H). Physically, we expect $L_{\max}$ to be at most about the local disk radius, r, so that E_{tot} is bounded.

Finally, let us consider the angular momentum transfer by the coronal magnetic field. The torque due to a single loop is given by

$$\Delta G(L, \theta) = -\frac{\Delta\Psi}{4\pi}\, |B_{\mathrm{hor}}|\, \frac{\Delta y\, \Delta r}{L} = -\frac{\Delta\Psi B_0}{8\pi}\, b_{\mathrm{top}}(L)\, L \sin 2\theta ,$$
(40)

and hence the total torque per unit disk area is

$$G = -\frac{\Delta\Psi B_0}{8\pi} \int\int dL\, d\theta\, \bar{F}(L, \theta)\, b_{\mathrm{top}}(L)\, L \sin 2\theta .$$
(41)

Let is again consider the truncated power-law example, $\bar{F} \sim L^{-\alpha(\theta)}$. For a fixed degree of anisotropy, e.g., a fixed the characteristic angular scale $|\sin\theta_{\min}|$ at which the function $\alpha(\theta)$ has a minimum $\alpha_{\min}$, the torque becomes dominated by large loops if $\alpha_{\min} < 3/2$, similar to E_{tot} [where we used equation (23]. It then scales as $L_{\max}^{3-2\alpha}$ and thus may become by a factor $(L_{\max}/H)^{3-2\alpha} \gg 1$ larger than the usual torque exerted directly by MRI turbulence within the disk, assuming that the magnetic field at the base of the corona is comparable to that in the disk. In reality, however, a decrease in $\alpha_{\min}$ may come hand-in-hand with an increase in the degree of anisotropy of the distribution function $\bar{F}(L, \theta)$ (see § 5.3), manifested as a simultaneous decrease in $|\sin\theta_{\min}|$. If this is the case, the torque amplification will be not as strong.

4. THE LOOP KINETIC EQUATION

In this section we discuss how to calculate the loop distribution function. In particular, we construct the loop kinetic equation that governs the evolution of this function.

4.1. Physical Assumptions of our Model

In order to build a quantitative model of the magnetic field in the corona, we need to make some specific assumptions about the most important physical processes that govern the life of individual coronal loops, including their interactions with each other. These assumptions are the main building blocks of our model; we shall discuss them in this section.

1) The Alfvén velocity in the corona is much faster than both the disk's rotational velocity at the given radius and the thermal velocity of the coronal gas; therefore, the corona is considered to be in a slowly-evolving force-free magnetostatic equilibrium at all times and almost everywhere (except for rapid rearrangements due to reconnection events, see below).

2) The disk is geometrically thin, with the gas scale-height much smaller than the distance from the central object, $H \ll r$. This gives us an important small parameter that can be used in the analysis. For example, this assumption gives us an "inertial range" of spatial scales much smaller than r but much larger than H. This enables us to perform an analysis that is local in r. In particular, this means that we can neglect geometrical effects resulting from cylindrical geometry when considering the flux-loop expansion process. Note, however, that the validity of the thin-disk assumption is questionable close to a black hole accreting near its Eddington limit.

3) The disk is differentially-rotating (e.g., keplerian). As a result, coronal loops with radially-separated footpoints are subject to continuous stretching in the toroidal direction. This generates toroidal magnetic field whose pressure inflates the loops and ultimately leads to the creation of a vertically-extended corona (see below).

4) At any given time, the shape and the overall height of each loop are determined by the magnetostatic equilibrium of the loop as if it were confined by a stratified atmosphere with certain external isotropic pressure $P(z)$. In turn, this pressure represents the effective magnetic pressure of all the neighboring loops, and we shall denote it as $P = \bar{B}^2(z)/8\pi$. This equilibrium shape is maintained at all times, since it adjusts on the Alfvén time scale, which is assumed to be much faster than the disk rotation.

5) The disk is turbulent due to the usual internal MRI (as opposed to coronal that may act simultaneously). The characteristic spatial scale of the turbulence is H, and the char-

acteristic time scale is Ω_K. The important effects of the disk turbulence on the corona are:

5a) *Flux Emergence* plays a very important role in the solar corona and, by analogy, is also believed to be important in the case of the disk Galeev et al. (1979). We generally expect the emerging magnetic loops to be relatively small in size (of order the disk thickness H) and to have typical magnetic fields of order $\alpha_{ss}^{1/2} B_{eq}$, where the dimensionless parameter $\alpha_{ss} \sim 0.01 - 0.1$ is the Shakura & Syunyaev (1973) viscosity coefficient and B_{eq} is the field strength that corresponds to equipartition with the gas pressure inside the disk. In addition, numerical studies of MRI turbulence show that the toroidal field in the disk tends to be larger than the radial field by a factor of 5-10. Thus, flux emergence is expected to be anisotropic, with newly emergent loops elongated in the toroidal direction by a factor of a few.

5b) Again, similar to the Sun, the disk turbulence leads to a two-dimensional random walk of the coronal loops' footpoints on the disk surface. We expect this random walk to be characterized by spatial and temporal scales of the order of H and Ω^{-1}, respectively. However, similar to the process of flux emergence discussed above, the random walk, in general, may be anisotropic, with characteristic steps in the azimuthal direction being somewhat larger than in the radial direction.

6) *Reconnection:* In our model, two loops may *reconnect* with each other, forming two new loops (see Fig. 5). Thus, reconnection represents a binary interaction between individual magnetic structures, analogous to binary collisions between particles in a gas.

We shall assume that, once triggered, a reconnection event (a flare) happens very quickly, essentially instantaneously on the orbital time scale. This assumption can be justified by noting that the corona is assumed to be a very low-density, and hence collisionless, environment. Therefore, reconnection there proceeds in the Petschek-like fast collisionless regime, enabled by anomalous resistivity or by the two-fluid (Hall-MHD) effects. The characteristic reconnection time-scale is then only by a factor of 10-100 slower than the Alfvén crossing time τ_A. Thus, since we assume that $V_A \gg V_K$, it is reasonable to expect that the typical duration of coronal reconnection events may still be fairly short compared with the orbital time-scale Ω^{-1}. Then, to the extent that Ω^{-1} is the main dynamical time-scale in our problem, characterizing differential rotation, flux emergence, and turbulent random walk, we can, for the purposes of our study, regard reconnection between loops, once triggered, as being essentially instantaneous. Thus, we arrive at a picture in which magnetic loops evolve slowly (*i.e.*, on the orbital time scale), but from time to time they suddenly and instantaneously reconnect. This picture is similar to the observed behavior of solar coronal loops, where the characteristic reconnection (or flare) time is typically much shorter than the typical loop lifetimes. Thus, from the standpoint of viewing the corona as an ensemble of many loops, reconnection events can be regarded as relatively infrequent binary collisions between loops, analogous to the binary collisions between particles in Boltzmann's gas. An important corollary from this is that the footpoints of the loops do not have time to move significantly during the reconnection event. As we shall see in § 4.2, this will give us the rules that determine the footpoint separations of newly-formed loops. We shall also assume that these newly-formed loops quickly assume their equilibrium shapes (see above).
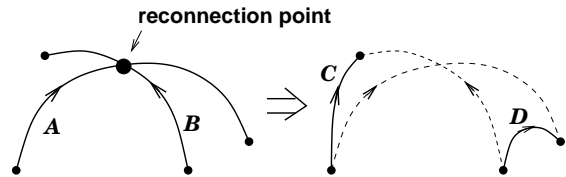

FIG. 5.— Reconnection between two loops as a binary process.

4.2. *The Loop Kinetic Equation*

Based on the above assumptions, we shall now work out an evolution equation for the loop distribution function F. We shall call this the *Loop Kinetic Equation* (LKE). This equation should have the following terms, reflecting the relevant physical processes:

1) Flux emergence/submergence acts as a source/sink of new coronal loops. It can be modeled by a source term, $S(\mathcal{A})$, that describes the rate at which the loops emerge into the corona, their characteristic sizes, magnetic field strengths, etc., (or, in a more elaborate model, by specifying the distributions of these quantities). Specifically, one can add loops at some characteristic "injection scale", somewhat larger than the disk thickness H, and remove very small loops, say, of size H or less, as it was done in the model by Hughes et al. (2003). In addition, in the ADC case, we expect flux emergence to be anisotropic, with the emerging loops being by a factor of a few longer in the toroidal direction than in the radial direction, as indicated by numerical simulations (*e.g.* Hirose et al. 2006).

An alternative way to take flux emergence into account is *via* the boundary conditions for F at small scales (of order H). This is the view adopted in our model. This choice is justified by arguing that the population of smallest loops comprising the "magnetic carpet" is predominantly determined by a detailed balance that is quickly established with the magnetic fields in the disk itself. This process turns over (operates) very quickly and hence the distribution of the very small loops is basically independent of what happens in the larger-scale corona.

2) Random footpoint motions due to the disk turbulence. Since we expect the characteristic steps of this random walk to be relatively small (of order H, see § 4.1) compared with the sizes of most loops under consideration, we can employ a Fokker–Planck-like approach to this process. This results in a diffusion operator with the diffusion coefficient of the order of the Shakura & Syunyaev (1973) α-viscosity coefficient: $D \simeq \alpha_{ss} c_s H \sim \alpha_{ss} \Omega H^2$. In general, however, this diffusion may be anisotropic, with D being a tensor (*e.g.*, a diagonal tensor with $D_{yy} > D_{rr}$). We expect the effect of the random walk to be relatively unimportant for large loops, $L \gg H$.

3) Keplerian differential rotation leads to a secular evolution of Δy,

$$\frac{d\Delta y}{dt} = -\frac{3}{2}\Omega\,\Delta r. \tag{42}$$

Here, $\Omega = \Omega_K(r)$ can be regarded as constant because we consider spatial scales that are small compared with the disk radius, $\Delta r \ll r$. In the Loop Kinetic Equation this process is described by an advection term, $(3/2)\Omega\,\Delta r(\partial F/\partial\Delta y)$.

4) Coronal MRI backreaction term $\dot{F}_{backreaction}$: in a geostrophic approximation, this is obtained by balancing the magnetic force on the footpoints (per unit area) with the Coriolis force (also per unit area) due to the rotation of the loop it

induces:

$$2\frac{B_z\mathbf{B}_{\text{hor}}}{4\pi} = 2\,\Sigma\,[\Omega \times \delta\mathbf{v}_{\text{backreaction}}]\,, \tag{43}$$

in which $\mathbf{v}_{\text{backreaction}}$ represents the departure from the keplerian rotation velocity.

5) Interaction of two loops by reconnecting with each other, yielding two new loops. This process is described by a binary collision term $\dot{F}_{\text{rec}}$. This is the most non-trivial term and we devote the entire next subsection (§ 4.3) to a detailed discussion of it.

At the end, we arrive at the following general form of the kinetic equation for the loop distribution function:

$$\frac{\partial F}{\partial t}(\Delta r, \Delta y, t) = S(\Delta r, \Delta y) + \left(D_{rr}\frac{\partial^2}{\partial \Delta r^2} + D_{yy}\frac{\partial^2}{\partial \Delta y^2}\right)F$$
$$+ \frac{3}{2}\,\Omega\Delta r\,\frac{\partial F}{\partial \Delta y} + \dot{F}_{\text{backreaction}} + \dot{F}_{\text{rec}} \tag{44}$$

The simplest meaningful case of this equation is when one neglects the source, diffusion, and feedback terms and looks for a *steady state* that is produced by the balance between Keplerian shear and reconnection:

$$\frac{3}{2}\,\Omega\Delta r\,\frac{\partial F}{\partial \Delta y} = \dot{F}_{\text{rec}}\,. \tag{45}$$

Our approach will thus be analogous to, and can be regarded as an extension of, the previous work by Tout & Pringle (1996), whose main goal was to study the formation of large magnetic structures *via* the reconnective "inverse cascade" in the corona. Following them, we also represent the coronal magnetic field by an ensemble of flux loops described by a distribution function. However, our model is more general and uses more realistic physics. We take into account a number of effects ignored in Tout & Pringle (1996), such as inflation of the loops as they are stretched by the Keplerian differential rotation. Also, in their model reconnection was taking place only at the disk surface and thus one of two newly reconnected loops was vanishingly small and was assumed to just disappear; as a result, the reconnection process did not conserve the number of loops. We, on the other hand assume that reconnection occurs higher in the corona, and hence two new loops form and the loop number is conserved (similar to the model by Hughes et al. (2003)).

4.3. *Reconnection Described as a Collision Integral*

Two loops $\mathcal{A}$ and $\mathcal{B}$ may interact by reconnecting with each other and forming two new loops $\mathcal{C}$ and $\mathcal{D}$ as a result (see Fig. 5). Following Tout & Pringle (1996), we shall describe this process by a nonlinear binary-collision integral, similar to the collision integral in the Boltzmann kinetic equation. In reality, of course, interaction between loops is more complicated and so such a description is oversimplified. Moreover, magnetic loops fill up the entire coronal space, and so they resemble more a non-ideal liquid rather than an almost ideal rarefied gas with infrequent binary encounters. Nevertheless, we believe that this binary-collision representation of reconnection can lead to some valuable physical insight into the complicated dynamics of the coronal magnetic field.

The Boltzmann collision integral can be split into two: the source term and the sink term. The sink term $\dot{F}_{\text{coll},-}(\mathcal{A})$ describes the rate of reduction in the number of loops of a given type $\mathcal{A}$ due to reconnection between these loops and all other loops. The source term $\dot{F}_{\text{coll},+}(\mathcal{A})$ describes the rate of increase in the number of loops of type $\mathcal{A}$ when they are a product of reconnection of other-type loops. By "type" we here mean a set of loops with the same values of their primary parameters (L, θ) or $(\Delta r, \Delta y)$. Thus, each of these terms is a quadratic integral operator, with a kernel that depends both on the types of the two loops and also on their relative position (see below). Thus, we can write the reconnection term schematically as

$$\dot{F}_{\text{rec}}(\mathcal{A}) = \dot{F}_{\text{rec},-}(\mathcal{A}) + \dot{F}_{\text{rec},+}(\mathcal{A})\,, \tag{46}$$

where

$$\dot{F}_{\text{rec},-}(\mathcal{A}) = -\int d\mathcal{B}\, Q_{\mathcal{AB}}\, F(\mathcal{A})\, F(\mathcal{B})\,, \tag{47}$$

$$\dot{F}_{\text{rec},+}(\mathcal{A}) = \frac{1}{2}\int\int d\mathcal{C}\, d\mathcal{D}\, Q_{\mathcal{CD}\to\mathcal{A}}\, F(\mathcal{C})\, F(\mathcal{D})\,. \tag{48}$$

Here, $d\mathcal{B} \equiv d\Delta r_B\, d\Delta y_B$, etc., The kernels $Q_{\mathcal{AB}}$ in the sink term and $Q_{\mathcal{CD}\to\mathcal{A}}$ in the source term are related *via*

$$Q_{\mathcal{AB}} = \frac{1}{2}\int d\mathcal{C}\, Q_{\mathcal{AB}\to\mathcal{C}}\,. \tag{49}$$

Using this relationship, the two terms can be combined as

$$\dot{F}_{\text{rec}}(\mathcal{A}) = \frac{1}{2}\int\int d\mathcal{C}\, d\mathcal{D}\, F(\mathcal{D})\left[Q_{\mathcal{CD}\to\mathcal{A}}\, F(\mathcal{C}) - Q_{\mathcal{AD}\to\mathcal{C}}\, F(\mathcal{A})\right]. \tag{50}$$

In order to go from this general expression to a specific operational procedure, we need to formulate the rules that govern the reconnection process. Indeed, the two new loops $\mathcal{C}$ and $\mathcal{D}$ formed as products of reconnection between two loops $\mathcal{A}$ and $\mathcal{B}$ cannot be arbitrary and certain selection rules must be applied. More specifically, from the assumption that reconnection is instantaneous on the orbital time scale, it follows that the footpoints of the reconnecting loops do not move significantly during the reconnection event. Only the way they are connected to each other changes. Therefore, the primary parameters (*i.e.*, footpoint separations) of loops $\mathcal{C}$ and $\mathcal{D}$ are uniquely determined by the footpoint positions of the two incoming loops $\mathcal{A}$ and $\mathcal{B}$:

$$\Delta r_C \equiv r_{C-} - r_{C+} = r_{A-} - r_{B+}\,, \tag{51}$$
$$\Delta r_D \equiv r_{D-} - r_{D+} = r_{B-} - r_{A+}\,, \tag{52}$$

and similarly for Δy_C, Δy_D. Here, A_+, A_- are the positive and negative polarity footpoints of the loop $\mathcal{A}$, *etc.* Mathematically, these rules play a role similar to the momentum and energy conservation conditions for particle collisions in kinetic theory of gases; they enter as δ-functions in the interaction integral in our loop kinetic equation. Thus, one can easily see that the parameters of the new loops depend not only on the parameters of the old loops, but also on the positions of $\mathcal{A}$ and $\mathcal{B}$ relative to each other (see below).

The kernel $Q_{\mathcal{AB}}$ in equation (47) is the probability rate (*i.e.*, probability per unit time) that two loops of types $\mathcal{A}$ and $\mathcal{B}$ will come together and reconnect. Thus, $Q_{\mathcal{AB}}$ describes the rate of reconnection events (the number of such events per unit time). This should not be confused with the concept of "reconnection rate", a widely-used term in reconnection research with a completely different meaning.

Now let us discuss on which physical parameters $Q_{\mathcal{AB}}$ should generally depend. Whereas Tout & Pringle (1996) just took $Q_{\mathcal{AB}} = \text{const}$, we want to develop a more realistic and more sophisticated model, taking into account several important factors. First, notice that $Q_{\mathcal{AB}}$ has dimensions of $[\text{cm}^2/\text{sec}]$. Based on dimensional arguments, it should then

be proportional to the characteristic rate at which the coronal magnetic field is reconfigured. In addition, it should also reflect the fact that larger loops have larger "interaction cross-section" (see below), and thus should be roughly proportional to the squares of loop sizes.

Let us first address the characteristic reconfiguration time-scale. The only fundamental dynamical time-scale in the corona, *i.e.*, the time-scale on which the corona, seen as an ensemble of elementary coronal structures, rearranges itself, is the orbital time, Ω^{-1} (or the inverse of the shear rate, $3/2\Omega$, which is not independent). This means that, if we represent the evolution by a sequence of discrete steps, each step representing a noticeable change in the relative position and/or orientation of the coronal elements, then the most appropriate choice for duration of these steps is of order Ω^{-1}. Therefore, in general, Q should scale with Ω. Next, if we follow a given magnetic element, at each new step there will be a certain probability $\kappa < 1$ that the resulting new magnetic configuration around this element becomes favorable for reconnection of this element with another. We shall treat κ as a constant number, independent of the loops primary parameters. Thus, the overall rate at which the loops are disrupted through reconnection with other elements should be proportional to $\kappa\Omega$:

$$Q_{\mathcal{AB}} = \kappa\,\Omega\,\sigma_{AB}\,, \qquad (53)$$

where we introduced the "reconnection cross-section" σ_{AB}.

The cross-section σ_{AB} should in some way scale with the loop sizes. It involves contributions from all possible relative positionings of the two interacting loops for which the two loops "effectively intersect". We shall describe this relative positioning by two impact parameters, $b_\parallel$ and $b_\perp$, defined as the offsets between the centers of the two loops in the direction parallel and perpendicular to loop $\mathcal{A}$, respectively. We shall assume that once the impact parameters are in a range such that the two loops "effectively intersect", the probability that these loops will reconnect is constant, independent of their positions or their parameters. Furthermore, for simplicity we shall assume $b_\parallel$ and $b_\perp$ to be uniformly-distributed independent random variables. Thus, σ_{AB} is just equal to the "interaction area" in the $(b_\parallel, b_\perp)$ space that corresponds to an "effective intersection" of the given two loops:

$$\sigma_{AB} = \int d\sigma_{AB} = \int\int db_\parallel\, db_\perp\,. \qquad (54)$$

But what do we mean by "effectively intersecting"? If the two loops are approximated by their central lines (one-dimensional objects), then the set of values $(b_\parallel, b_\perp)$ for which they intersect is also one-dimensional (a line segment), and thus has measure zero in the two-dimensional $(b_\parallel, b_\perp)$ space. In other words, the probability that two randomly-drawn lines intersect is zero in the three-dimensional space. Therefore, to get a meaningful result, we need to take into account finite thicknesses of the loops. In particular, we shall say that two loops "effectively intersect" when the closest distance between their central lines is less than a certain fraction of the combined loop thicknesses at the intersection height. Operationally, for a given value of $b_\parallel$, say, we can introduce the y-cross-section $\sigma_{AB,\perp}(b_\parallel)$ as the spread in the values of $b_\perp$ which result in an effective intersection of two given loops $\mathcal{A}$ and $\mathcal{B}$. We can then write

$$\sigma_{AB} = \int \sigma_{AB,\perp}(b_\parallel)\, db_\parallel\,. \qquad (55)$$

where the integral is taken over the range of impact parameters $b_\parallel$ for which an intersection between loops $\mathcal{A}$ and $\mathcal{B}$ is at all possible.

Correspondingly, the sink-term part of the reconnection integral can be written as

$$\dot{F}_{\rm rec,-}(\mathcal{A}) = -\kappa\Omega \int\int d\mathcal{B}\, db_\parallel\, \sigma_{\mathcal{AB},\perp}(b_\parallel)\, F(\mathcal{A})\, F(\mathcal{B})\,. \quad (56)$$

Now let us consider the source term (48). Employing the arguments given earlier in this subsection, we introduce the cross-section for two given loops $\mathcal{C}$ and $\mathcal{D}$ to reconnect giving a loop $\mathcal{A}$ as a result: $Q_{\mathcal{CD}\to\mathcal{A}} = \kappa\,\Omega\,\sigma_{CD\to A}$. We can then write

$$\dot{F}_{\rm coll,+}(\mathcal{A}) = \frac{\kappa\Omega}{2} \int\int d\mathcal{C}\, d\mathcal{D}\, \sigma_{\mathcal{CD}\to\mathcal{A}}\, F(\mathcal{C})\, F(\mathcal{D})\,. \qquad (57)$$

The $\mathcal{D}$ integral in this equation is taken over all the loops that can yield a loop of type $\mathcal{A}$ as a result of reconnection with a loop of a given type $\mathcal{C}$. Note that, whereas one did not need to know reconnection product loops to compute the sink term (56), in order to calculate the source term, this knowledge is in fact necessary. It is contained in our "reconnection rules", such as those given by equations (51)–(52). For definiteness, let us consider the case when the resulting loop $\mathcal{A}$ starts from the "+" footpoint of loop $\mathcal{C}$ and ends at the "-" footpoint of loop $\mathcal{D}$. Then, for given $\mathcal{C}$ and $\mathcal{A}$, there is a well-defined range of impact parameters $b_\parallel$ for which one can find one (or sometimes two) loop $\mathcal{D} = \mathcal{D}_{\mathcal{A}-\mathcal{C}}(b_\parallel)$ that intersects loop $\mathcal{C}$ and ends at the end footpoint of loop $\mathcal{A}$. Thus, in principle, for a given $b_\parallel$ one can formulate the rules that relate the primary parameters Δr_D and Δy_D to those of loops $\mathcal{C}$ and $\mathcal{A}$. We shall denote these relationships by $\Delta r_D^{A-C}(b_r)$ and $\Delta y_D^{A-C}(b_\parallel)$. In general, there may be one or two such solutions.

Recalling now that flux tubes have a finite thickness, we have, by analogy with equation (55),

$$\sigma_{CD\to A} = 2 \int db_\parallel\, \sigma_{CD,\perp}(b_\parallel)\, \delta[\mathcal{D} - \mathcal{D}_{\mathcal{A}-\mathcal{C}}(b_\parallel)]\,, \qquad (58)$$

where $\delta[\mathcal{D} - \mathcal{D}_{\mathcal{A}-\mathcal{C}}(b_\parallel)] \equiv \delta[\Delta r_D - \Delta r_D^{A-C}(b_\parallel)] \times \delta[\Delta y_D - \Delta y_D^{A-C}(b_\parallel)]$. The factor 2 accounts for the fact that in the preceding paragraph we considered only one half of all possible configurations, requiring the starting footpoint of loop $\mathcal{A}$ to be the starting footpoint of loop $\mathcal{C}$. For each such configuration there will also be an identical contribution from interchanging loops $\mathcal{C}$ and $\mathcal{D}$.

Substituting this cross-section into our expression (57) for $\dot{F}_{\rm coll,+}(\mathcal{A})$, and using the δ-function to integrate over $d\mathcal{D} = d\Delta r_D d\Delta y_D$, we get

$$\dot{F}_{\rm coll,+}(\mathcal{A}) = \kappa\,\Omega \int\int d\mathcal{C}\, db_\parallel\, \sigma_{CD_{A-C},\perp}(b_\parallel)\, F(\mathcal{C})\, F[\mathcal{D}_{\mathcal{A}-\mathcal{C}}(b_\parallel)]\,. \qquad (59)$$

Combining equations (56) and (59), we can write:

$$\dot{F}_{\rm rec}(\mathcal{A}) = \kappa\,\Omega \int\int d\mathcal{C}\ db_\parallel\, F(\mathcal{C})$$
$$\times \left[F[\mathcal{D}_{\mathcal{A}-\mathcal{C}}(b_\parallel)]\sigma_{CD_{A-C},\perp}(b_\parallel) - F(\mathcal{A})\sigma_{AC,\perp}(b_\parallel) \right] \quad (60)$$

Effect of Finite Loop Thickness

For a given value of $b_\parallel$, one first finds the coordinates $[r(b_\parallel), y(b_\parallel), z(b_\parallel)]$ of the point where the central lines of the two loops would intersect. After that, one calculates the $\perp$-extent of each of the two loops at this point, which hence gives one $\sigma_{AB,\perp}(b_\parallel)$.

When doing this, one should take into account the following important effect. If the loops have no internal twist, as we assume here, the longitudinal magnetic field is approximately constant across a loop and is roughly equal to the characteristic magnetic field $\bar{B}(z)$ at a given height z. Then, by flux conservation, the cross-section of the loop (normal to its central line) varies along its length, and, in particular, may increase greatly at large heights if $\bar{B}(z)$ drops off rapidly. More precisely, approximating a loop's cross-section at a given height z as a circle of some radius $d(z)$, we can estimate this radius as $d(z) \sim [\Delta\Psi/\pi\bar{B}(z)]^{1/2} = d_0[\bar{B}(z)/B_0]^{-1/2}$. As long as the loop is slender, $d \ll L$, this should be a good approximation. Thus, if the intersection point lies high above the disk, so that $\bar{B}(z) \ll B_0$, the characteristic loop thickness is much larger than near the disk surface. Consequently, the reconnection cross-section is increased, which has important implications for the "inverse cascade" of magnetic loops in the corona. It is also interesting to note that this process is controlled by the self-consistent field $\bar{B}(z)$.

[Note that, in the case of twisted loops this effect is not as profound and a more accurate approximation is probably given by $d(z) \simeq d_0 = $ const (see § 6.2).]

Thus, typically we expect $\sigma_{AB,\perp}$ to scale as

$$\sigma_{AB,\perp}(b_\parallel) \sim 2\,d[z(b_\parallel)] \sim 2\sqrt{\frac{\Delta\Psi}{\pi\bar{B}[z(b_\parallel)]}} \sim 2\,d_0\sqrt{\frac{B_0}{\bar{B}[z(b_\parallel)]}}\,.$$
(61)

For example, if $\mathcal{B}$ is the smaller of the two loops, we expect the typical interaction height to be of the order of this loop's height Z_B. Correspondingly, we expect $\sigma_{AB,\perp} \sim d_0 b^{-1/2}(Z_B)$, where $b(z) \equiv \bar{B}(z)/B_0$. This estimate for $\sigma_{AB,\perp}(b_\parallel)$ will be roughly valid for almost the entire allowed range of $b_\parallel$, which is of order $4\,\Delta r_B$.

To sum up, larger loops have larger cross-sections for reconnection, for two complementary reasons. First, the cross-section is enhanced because larger loops have larger range of impact parameters (in the radial direction, say) for which intersection of their central lines is possible. Second, larger loops extend to, and may interact at, larger heights, where the mean magnetic field is weaker and hence where the loops become fatter. They thus have a greater chance of overlapping with each other. As a result, the reconnection cross-section scales with the size L_B of the *smaller* of the two loops as

$$\sigma_{AB} \sim L_B\,d_0\,b^{-1/2}(Z_B)\,,$$
(62)

[for $L_B \gg d(Z_B)$]. We thus see that the function $\bar{B}(z)$ affects the evolution of the loop distribution function. Since, according to § 3.2, $\bar{B}(z)$ is itself determined by the distribution function, this means that determining these two functions together in a self-consistent way requires an iterative procedure.

What is important here, is that larger loops have a tendency to reconnect with each other quickly, probably leading to a rapid "inverse cascade" to even larger loops. In addition, the fact that reconnection with large loops cannot be neglected suggests that a Fokker-Planck-like approximation to the reconnection term will not work. This is because reconnection events that lead to large changes in loop parameters are important and so our collision integral cannot be described by a differential diffusion-like operator.

5. NUMERICAL SOLUTION

5.1. *Numerical Setup*

We solve the LKE numerically and obtain a steady state solution. For simplicity we leave out the turbulent diffusion term, the coronal backreaction term, and the source term (flux emergence is then treated *via* the boundary condition at small scale, see § 5.2). Thus, we include only the two processes which we believe are the most important: Keplerian shear and reconnection between loops. Correspondingly, we aim here at investigating the effect of the relative importance of these two processes on the steady-state loop distribution function.

In the numerical implementation we work in the (L,θ) parameter space where $L = (\Delta r^2 + \Delta y^2)^{1/2}$ is the distance between the footpoints and θ is the angle the vector $(\Delta r, \Delta y)$ makes with the toroidal direction, measured clockwise: $\tan\theta = \Delta r/\Delta y$. We use a grid that is uniform in θ (between 0 and 2π) but logarithmic in L. The L grid spans from $L_{\min} = 1$ to some $L_{\max} \gg 1$ (usually we take $L_{\max}$ to be 10 or 20) in length units such that $H \simeq 1$.

The advection term resulting from Keplerian shear is very easy to implement, we just use one-sided derivatives.

The reconnection collision integral is obviously more complicated and we devote the rest of this subsection to our numerical implementation of it. At each time step we go over all possible pairs of loops $\mathcal{A}$ and $\mathcal{B}$. Furthermore, for each given pair we go over all possible reconnecting configurations, distinguished by the impact parameter $b_\parallel$, defined as the displacements between the centers of the two loops in the direction along loop $\mathcal{A}$ (see § 4.3). Thus, at each timestep, we are performing a five-dimensional (5D) integration, which makes increasing resolution extremely numerically costly. We found, however, that numerical convergence is very good and relatively modest resolution suffices. To study numerical convergence, we performed calculations with $N_L = 20$ and 40 points in $\log L$, $N_\theta = 20$, 40, 60, and 80 points in θ, and 30, 50, or 100 points in $b_\parallel$. We found the resulting $F(L,\theta)$ to be essentially unchanged, although small values of κ required a higher θ-resolution for convergence (see below).

For simplicity, in our treatment of reconnection, we assume the loops to be *semi-circular* in shape, instead of using equilibrium shapes discussed in § 3.1. This simplification has two benefits. First, since the shapes are described by relatively simple analytical expressions, we can derive explicit analytical relationships expressing the parameters of the two product loops in terms of the parameters of the interacting loops and the impact parameter (we call these relationships the "reconnection rules"). Having such expressions in an explicit form greatly simplifies the numerical procedures.

The second advantage of the semicircular approximation stems from the observation that, because all the loops have the same shape, the reconnection rules essentially depend only on the ratio of loop sizes, whereas their dependence on the absolute loop size is a trivial rescaling. Likewise, the reconnection process is, by itself, isotropic, *i.e.*, does not depend on the absolute orientation of the loops, only on the angle between them. This enables us to to reduce the analysis of reconnection between two given loops $\mathcal{A}$ and $\mathcal{B}$ to considering a template that corresponds to the given angle between the loops and the given length ratio L_B/L_A. That is, we can analyze reconnection between any two loops in a rotated and rescaled system of coordinates, (x',y'), in which one of the loops (loop $\mathcal{A}$ for definiteness) is in the positive x'-direction, *i.e.*, has $\theta'_A = \pi/2$ and has unit length, $L'_A = 1$. In practice, we first (even before we start the evolution of LKE), create a lookup table describing the reconnection rules for interac-

tion of this loop $\mathcal{A}'$ with all other loops $\mathcal{B}'$. The lookup table is 3D, two of the coordinates being θ'_B and L'_B, and the third coordinate being the rescaled impact parameter $b'_\parallel$; the latter lies within the range from $-(1+\Delta x'_B)/2$ to $(1+\Delta x'_B)/2$, where $\Delta x'_B = L'_B \sin\theta'_B$. For each given θ'_B, L'_B and $b'_\parallel$, it is just a matter of simple algebra to figure out the perpendicular displacement $b'_\perp$ corresponding to the intersection between the semi-circular loops. Simultaneously one finds the 3D position of the intersection point between loops $\mathcal{A}'$ and $\mathcal{B}'$ for given $b'_\parallel$ (including the height of the reconnection point). One can then readily deduce the parameters of the two product loops $\mathcal{C}'$ and $\mathcal{D}'$. It is easy to see that the problem reduces to quadratic equations and hence for each θ'_B, L'_B, and $b'_\parallel$ there may be zero, one, or two solutions.

During the time evolution we use this table as follows. For each given pair of loops $\mathcal{A}$ and $\mathcal{B}$ we find their corresponding template pair by rotating them by $\theta_A - \pi/2$ and rescaling the loop sizes by L_A. We also rescale the impact parameter by L_A, i.e., $b'_\parallel = b_\parallel/L_A$. We then use the template table to find the two template product loops and we transform them back by multiplying by L_A and rotating by $\pi/2 - \theta_A$ to find the actual product loops $\mathcal{C}$ and $\mathcal{D}$. Having a grid uniform in θ and $\log L$ makes this procedure especially convenient and straightforward.

Once the product loops are found, one also needs to figure out the reconnection cross-sections corresponding to given $\mathcal{A}$, $\mathcal{B}$, and $b'_\parallel$. In accordance with the above discussion, $d\sigma_{AB}(b'_\parallel)$ is proportional to $db_\parallel = L_A(1+\Delta x'_B)/N_b)$ and to the loop combined deprojected thickness $db'_\perp$ at the intersection point. Apart from simple geometrical projection factors, $db'_\perp$ is proportional to $d(z) \sim d_0[B_0/\bar{B}(z)]^{1/2}$, where z is the height of the reconnection point above the disk. This factor enhances the reconnection probability for large loops intersecting at large heights. Since $\bar{B}(z)/B_0$ itself depends on $F(L,\theta)$, this procedure requires iteration. Once the reconnection cross-section $\sigma_{AB}(b'_\parallel)$ is found, one can proceed to evolve the number of incoming ($\mathcal{A}$ and $\mathcal{B}$) and product ($\mathcal{C}$ and $\mathcal{D}$) loops. Namely, $F(\mathcal{A})d\mathcal{A}$ and $F(\mathcal{B})d\mathcal{B}$ are reduced by

$$F(\mathcal{A})\,F(\mathcal{B})\,d\mathcal{A}\,d\mathcal{B}\,L_A\,db'_\parallel\,\kappa\,\Omega\,\sigma_{AB}(b'_\parallel)\,\Delta t\,, \qquad (63)$$

and $F(\mathcal{C})d\mathcal{C}$ and $F(\mathcal{D})d\mathcal{D}$ are increased by the same amount at each timestep Δt.

Finally, we varied the initial conditions and found that our resulting steady state solutions are insensitive to them.

5.2. Boundary Conditions

For various physical reasons, we expect our model to break down at both small scales and large scales. We thus need to discuss how to prescribe the boundary conditions for the LKE at both of these scales.

At small scales, $L \sim H$, the model is expected to become invalid because the magnetic field is no longer force-free, as plasma pressure starts to become dynamically important at small heights. In addition, the characteristic thickness of magnetic structures near the disk surface is expected to be of order H and hence small loops with $L \sim H$ are not going to remain slender as our model assumes. Thus we need to understand what is a plausible way to describe these small loops. At small scales the dynamics of magnetic loops is strongly affected by rapid flux-exchange (e.g. flux-emergence) processes with the turbulent disk. One can therefore argue that the overall distribution of the smallest loops is largely determined by the detailed balance equilibrium that is rapidly established between smallest loops and the turbulent disk. Characterizing

this intense interaction with the disk turbulence and calculating the small-scale distribution function is completely beyond our present model. It would require thorough understanding of 3D MHD turbulence in stratified disks with simultaneous actions of the MRI and Parker instability (Tout & Pringle 1992); most likely, this task will be accomplished using sophisticated numerical simulations. However, what matters for our model here is that we expect that the number of small loops be essentially insensitive to what happens to larger coronal loops. This means that we can mimic the disk-corona interaction by setting-up a Dirichlet-type boundary condition at small scales, i.e., by prescribing the distribution function at some small-cutoff scale $L_{\min} \sim H$:

$$F(L = L_{\min}, \theta) = F_1(\theta)\,. \qquad (64)$$

(In our model we set $L_{\min} = 1$.) Notice that $F_1(\theta)$ is in general expected not to be isotropic because emerging loops will be preferentially azimuthally elongated ($|\sin\theta| \ll 1$). In the present simulations, however, we take it to be isotropic, $F_1(\theta) = $ const.

Our model also breaks down at large scales. In particular, when a loop's size becomes comparable to the disk radius r, the local cartesian geometry adopted here is no longer applicable, and toroidal effects become important. This leads to a much faster expansion of stretched loops, resulting in a complete opening of the field, as discussed in § 2.2. In the future, we plan to implement a physically realistic way of treating the opening of large loops by incorporating open field lines into our model (see § 6.3).

In the present model, however, we just introduce some large cut-off scale, $L_{\max}$, and we set boundary conditions at this scale. We experimented with two types of boundary conditions: in one case, we set $F(L_{\max}) = 0$, i.e., we simply remove all loops that reach the cut-off scale. In the other case, we just limit the growth of loops beyond $L_{\max}$; i.e., as soon as a loop's length exceeds $L_{\max}$, we reset it back to $L_{\max}$. This leads to a gradual pile-up of loops near $L_{\max}$, but does not affect the loop distribution on smaller scales; in particular, it does not change the power law tail for sizes just slightly smaller than $L_{\max}$.

5.3. Results

Distribution Function

We performed a series of calculations with several different values of κ ($\kappa = \infty$, 1, 0.3, 0.1, 0.03, 0.02, 0.01, 0.005, and 0.003). Some of the resulting steady state loop distribution functions for our fiducial resolution $N_L = 40$, $N_\theta = 80$ and for the large-scale boundary condition $F(L_{\max}, \theta) = 0$, $L_{\max} = 10$, are presented in Figures 6–8. In particular, Figures 6 and 7 show (in log-log coordinates) F as a function of L for purely radial loops ($\theta = \pi/2$) and purely toroidal loops ($\theta = 0$), respectively. In the case $\kappa = \infty$ (keplerian shear turned off), the distribution function is isotropic. This is of course expected, since loop-loop reconnection — the only process determining the distribution function in this case — by itself is independent of the absolute orientation of the reconnecting loops. As the frequency of reconnection events relative to shear, quantified by κ, is decreased, a given loop (especially if it has a large $|\Delta r|$) experiences, on average, larger stretching in the toroidal direction by the shear before it undergoes reconnection with another loop. As a result, the loops become predominantly azimuthal and the loop distribution function becomes more and more anisotropic: $F(\theta = \pi/2, L)$ steepens, whereas $F(\theta = 0, L)$ becomes shallower with decreasing κ.
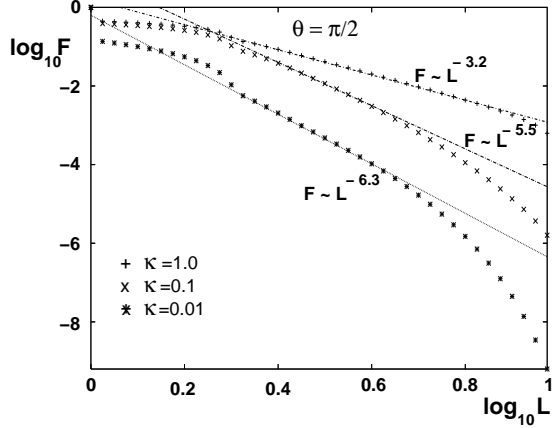
FIG. 6.— Distribution function for purely radial loops ($\theta = \pi/2$), for dimensionless reconnection parameter $\kappa = 1.0$ (pluses), 0.3 (crosses), and 0.1 (asterisks).
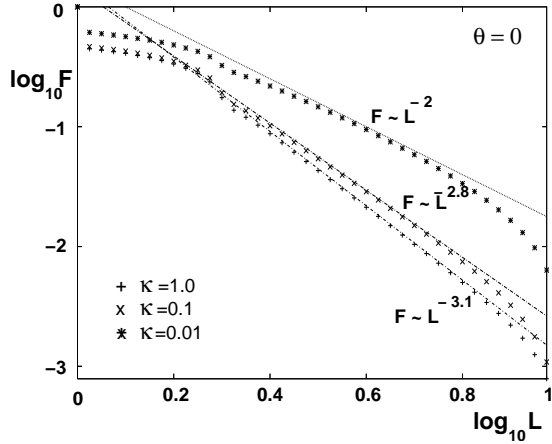

FIG. 8.— Power-law exponent $\alpha_\kappa(\theta)$ for $\kappa = 1.0$, 0.3, 0.1, 0.03.

The dependence of the power-law exponent $\bar{\alpha}$ on the reconnection parameter κ is plotted in Figure 10. We find that when reconnection is strong compared with keplerian shear ($\kappa \gtrsim 0.2$), the power-law exponent stays close to 3.1, independent of κ. This is because, as long as the keplerian shear can be neglected, reconnection is the only term on the right-hand side of the LKE. In this case, κ cannot affect the steady state solution, it can only regulate how fast this solution is achieved. As κ is decreased, however, the keplerian shear term becomes important and $\bar{\alpha}(\kappa)$ starts to decrease. We find that its overall behavior can be approximated by $\bar{\alpha}(\kappa) \simeq 3.1 =$ const for $\kappa \gtrsim 0.2$ and $\bar{\alpha}(\kappa) \simeq 3.55 + (1/3)\ln\kappa$ for $\kappa \lesssim 0.2$. Correspondingly, we expect $\bar{\alpha}(\kappa)$ to crosses the critical values 2 and 3/2 (see § 3.4) at $\kappa_2 \simeq 0.01$ and $\kappa_{3/2} \simeq 0.002$, respectively. As a reminder, $\bar{\alpha} < 3/2$ means that the total magnetic energy of the corona is dominated by the largest loops.

FIG. 7.— Distribution function for purely toroidal loops ($\theta = 0$), for $\kappa = 1.0$ (pluses), 0.1 (crosses), and 0.01 (asterisks).

Because our problem lacks a preferred length-scale between $L_{\min}$ and $L_{\max}$, we find that, along each ray $\theta =$ const, $F(L)$ is well described by a power law with the orientation-angle-dependent exponent:

$$F(L, \theta) \sim L^{-\alpha_\kappa(\theta)}. \qquad (65)$$

Figure 8 presents the function $\alpha_\kappa(\theta)$ for $\kappa = 1$, 0.3, 0.1, and 0.03.

Finally, in order to estimate the total magnetic energy in the corona and the total magnetic torque (see § 3.4), one needs to know the θ-integrated distribution function,

$$\bar{F}(L) \equiv \int_0^{2\pi} F(L, \theta)\, d\theta. \qquad (66)$$

In Figure 9 we plot $\bar{F}(L)$ for $\kappa = 1.0$, 0.3, 0.1, 0.03, 0.01, and 0.005 in log-log coordinates. In general, of course, one cannot expect a θ-integral of exponents $L^{-\alpha(\theta)}$ to be itself a power law of L. However, we find that the integral is strongly dominated by the range of values θ corresponding to the ridge in $F(L, \theta)$, and so a power law $\bar{F}(L) \sim L^{-\bar{\alpha}(\kappa)}$ is actually a reasonably good approximation, especially for relatively large values of κ. Because the power-law fit is not ideal, there is some degree of uncertainty in determining the value of $\bar{\alpha}$; we estimate the characteristic error to be $\lesssim 0.1$.
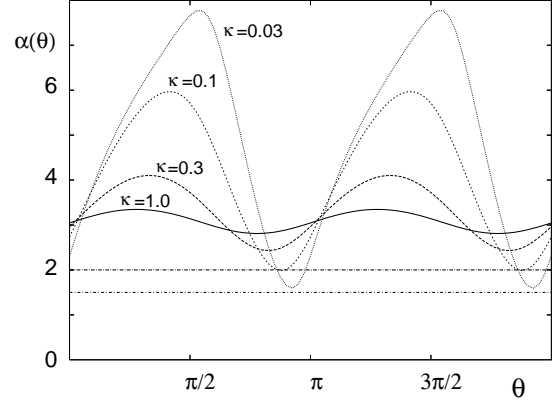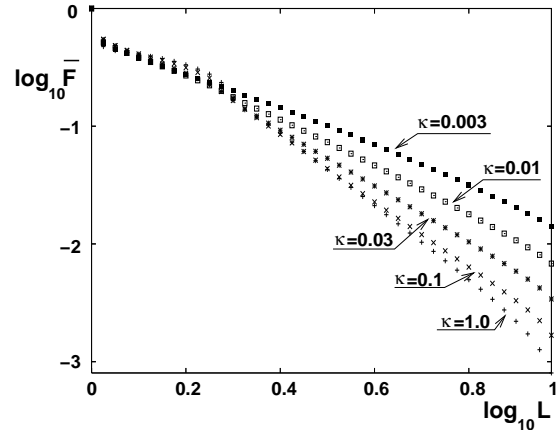

FIG. 9.— Orientation-averaged loop distribution function $\bar{F}(L)$ for $\kappa = 1.0$, 0.3, 0.1, 0.03, 0.01, and 0.005.

Finally, although most of our runs were done with $L_{\max} = 10$, we also conducted some runs with $L_{\max} = 20$. We found the distribution function to be essentially the same; the power-law just extended further in the $L_{\max} = 20$ case but the slope and the normalization were unchanged.

Energetics and Torque

Using the computed loop distribution functions, we calculate the magnetic energy density as a function of height above
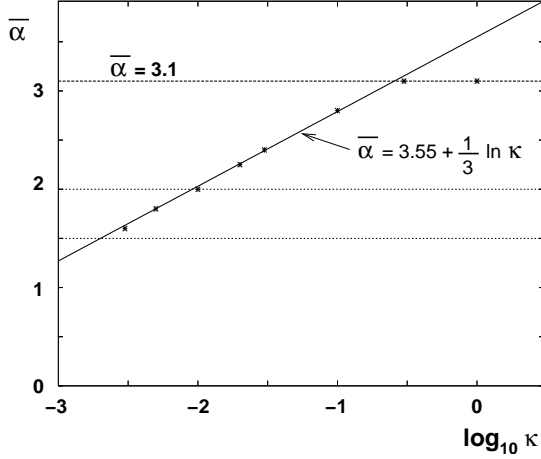
FIG. 10.— Power-law exponent $\bar{\alpha}$ for the orientation-averaged loop distribution function $\bar{F}(L) \sim L^{-\bar{\alpha}}$, as a function of κ. The dotted horizontal lines at $\bar{\alpha} = 2$ and $\bar{\alpha} = 3/2$ correspond, respectively, to the critical values at which the magnetic energy of the largest loop, $\mathcal{E}(L_{\max})$, and the total magnetic energy in the corona, $E_{\rm tot}$, start to become dominated by the large-scale cut-off $L_{\max}$ (see § 3.4).

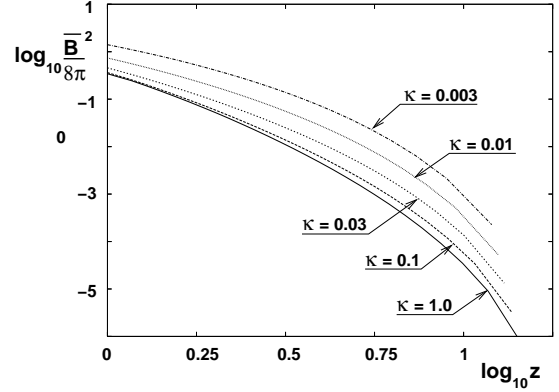

FIG. 11.— Magnetic energy density as a function of height, $\bar{B}^2(z)/8\pi$, for several values of the dimensionless reconnection parameter κ.
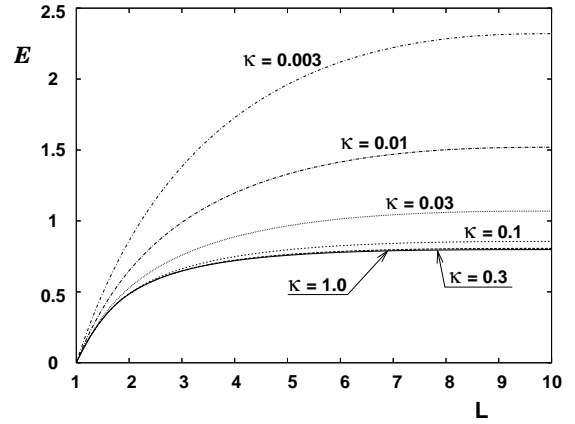

FIG. 12.— Energy associated with a loop of length L, $\mathcal{E}(L)$, for several values of the dimensionless reconnection parameter κ.
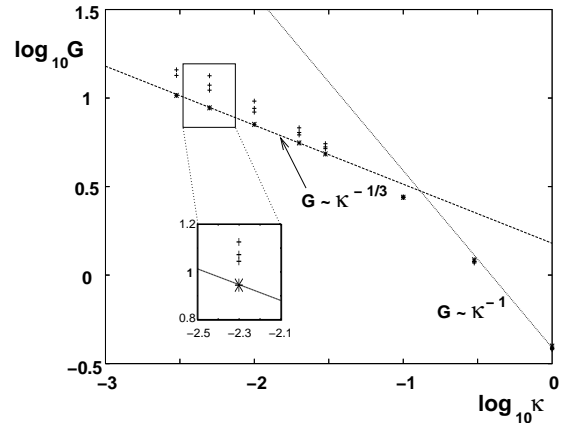

FIG. 13.— Coronal magnetic torque G (normalized to $\Delta\Psi^2/4\pi$) as a function of κ in logarithmic coordinates. The small insert shows an expanded view of convergence with respect to the resolution in the θ direction for $\kappa = 0.005$ ($\log_{10}\kappa = -2.3$). The plus signs mark the values obtained with $N_\theta = 40$, 60, and 80 (top to bottom) and the asterisks correspond to the extrapolation to $N_\theta = \infty$.

the disk, $\bar{B}^2(z)/8\pi$, and the energy of a loop as a function of its length, $\mathcal{E}(L)$, for several different values of κ (see Figs. 11 and 12). We see that these functions remain essentially independent of κ as long as it is large enough, $\kappa \gtrsim 0.1$), but start changing for smaller values of κ. In particular, we find that for a given value of κ, $\mathcal{E}(L)$ saturates to a finite value at large L. This is because, although a large loop occupies a relatively large volume at large z, the magnetic energy density very high above the disk is very low, and so the contribution of the large-z part of a loop to its total energy is relatively small. However, we find that the asymptotic value of $\mathcal{E}(L)$ at large L begins to increase rapidly as κ is lowered below roughly $\kappa_2 \simeq 0.01$, in agreement with the expectations of § 3.4.

We also calculate the total torque G, transmitted by the coronal magnetic field and the total magnetic energy in the corona, $E_{\rm tot}$. We show these quantities as functions of κ in Figures 13 and 14. Since our code is only first-order accurate with respect to the number N_θ of grid points in the θ direction, the finite θ-resolution becomes an issue at very small values of κ, where the distribution function is strongly anisotropic. Therefore, to get more accurate values for the torque and the magnetic energy corresponding to $N_\theta = \infty$, we use linear extrapolation based on the calculations with $N_\theta = 40$, 60, and 80, separately for each value of κ (see Figs. 13 and 14).

We find that, as κ is decreased, the coronal angular momentum transfer $G(\kappa)$ increases steadily as κ^{-1} for $\kappa \gtrsim 0.1$, as is expected due to the increased degree of anisotropy of the loop distribution function. As κ becomes $\lesssim 0.1$, further growth of $G(\kappa)$ slows down and becomes $G \sim \kappa^{-1/3}$. The fact that $G(\kappa)$ is a power law in this range is understandable in light of the discussion at the end of § 3.4, combined with the logarithmic dependence of $\bar{\alpha}(\kappa)$ reported above. We also find that the total magnetic energy in the corona, $E_{\rm tot}(\kappa)$, is nearly flat for large values of κ, but starts to increase roughly as $\kappa^{-1/2}$ as κ is lowered below $\kappa \lesssim 0.05$ (see Fig. 14).

Furthermore, in agreement with the discussion in § 3.4, we find that both the magnetic torque and the total magnetic energy are substantially larger in the $L_{\max} = 20$ case than in the $L_{\max} = 10$ case for small values to κ, whereas they are essentially the same for both values of $L_{\max}$ for larger κ.

6. DISCUSSION

There are several extensions of our model that we plan to develop in the near future. They include: (1) characterizing the coronal field backreaction on the disk motions; (2) including open magnetic flux; (3) taking into account mag-
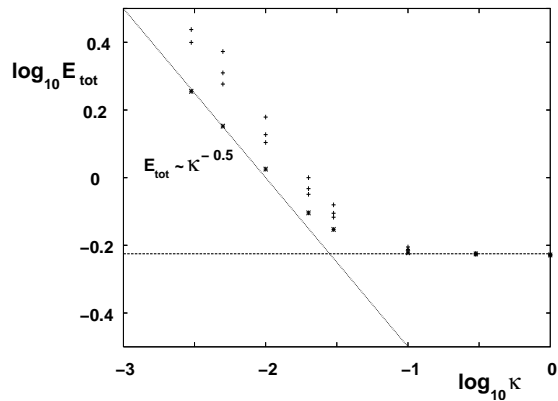
FIG. 14.— Total coronal magnetic energy (normalized to $\Delta\Psi^2/4$) as a function of κ in logarithmic coordinates. As in Figure 13, the plus signs correspond to $N_\theta = 40$, 60, and 80 (top to bottom) and the asterisks corresponds to the extrapolations to $N_\theta = \infty$, for each κ.

netic twist inside the loops; (4) incorporating a more realistic prescription for reconnection; (5) investigating the mass exchange between the disk and the corona and its effect on regulating coronal energy release; (6) studying the interaction between the coronal magnetic field and a super-imposed external large-scale field; (7) assessing the implications of our theory for observations, *e.g.*, in terms of time delay between hard and soft X-ray emission. We discuss some of these issues in more detail in this section.

6.1. *Open Flux Tubes, Outflows, and Net Vertical Flux*

In this paper we have assumed that closed loops are the only magnetic structures in the corona. In principle, however, one should also consider a population of open flux tubes. If considered to be force-free along their entire (infinite) length, open loops exert no torques on the disk (in the non-relativistic limit) but contribute to the averaged magnetic pressure $\bar{B}^2(z)$ everywhere and thus prevent it from becoming too small at large heights. Open tubes are also essential for investigating the role of the corona in launching large-scale outflows; relaxing the assumption of force-free fields allows the inertia of the outflow to exert a torque on the disk along open field lines (Blandford & Payne 1982) by analogy with the angular-momentum loss of the Sun to the solar wind (Weber & Davis 1967).

In our model, open loops could be introduced through the large-scale cut-off for the closed loops. That is, whenever a closed loop grows to exceeds a certain maximal footpoint separation L_{max}, it could be replaced by a pair of open flux tubes of opposite polarities. The large-scale cut-off may be physically associated with the disk radius, *r*. It should determine the fraction of magnetic flux that is open at any given time. The rules that govern the interaction of open tubes with closed ones and with themselves, are straightforward: two open tubes of the same sign do not interact; two open tubes of opposite sign can annihilate by reconnection, forming one single closed loop. An open tube can also reconnect with a closed loop, forming again an open tube of the same sign and a new closed loop.

In addition to such pairs of positive and negative open flux tubes, there may also be a net vertical magnetic flux imposed on the disk by the central object or the ambient inter-stellar medium. The radial transport of such externally-imposed field across a turbulent accretion disk is an im-

portant problem with significant consequences for understanding the different spectral states of accreting black holes (Spruit & Uzdensky 2005), for production and collimation of disk-driven winds and jets, and for star–disk magnetic interaction (*e.g.* Uzdensky et al. 2002a,b), which is believed to regulate the spin evolution of accreting neutron stars in X-ray pulsars (Ghosh & Lamb 1978), as well as young stars (Königl 1991; Matt & Pudritz 2005). This problem, however, is highly non-trivial (*e.g.* Lubow & Spruit 1995; Heyvaerts et al. 1996; Livio et al. 1999; Spruit & Uzdensky 2005), in part because the effective transport of the large-scale open flux may be greatly affected by reconnection with the small- and intermediate-scale closed coronal magnetic loops (Spruit & Uzdensky 2005; Fisk 2005). Incorporating a net large-scale flux into our statistical model is very straightforward and its overall transport should come out automatically. We therefore believe that our theoretical model can be a very useful tool for addressing this problem.

6.2. *Twisted Loops*

In this paper we have assumed, for simplicity, that coronal loops have no longitudinal current, and hence have no internal twist. In a more general situation, however, there may be force-free field-aligned currents along the loops, generated in response to certain disk footpoint motions: specifically, rotation of field-line footpoints around each other.

Internal twist would have two major consequences for our coronal model. First, the pinch force of the associated longitudinal current (parallel to the magnetic field because of the force-free assumption) will tend to reduce the width of loop and its cross section for reconnection with other loops. One might consider as a limiting case that the effective thickness of the loop is constant along its length. There is indeed observational evidence that in the solar corona bright loops usually have a nearly constant thickness along their length Klimchuk (2000).

Second, if the loop twist becomes too large, then the entire loop may become kink-unstable and, as a result, the loop makes a transition to a different equilibrium, where the internal twist is partially transformed into the global writhe of the loop. That is, the loop no longer lies in one plane but rather has a twisted, helical shape. Such *S*-like loops (so called sigmoidal loops) are routinely observed in the solar corona (Rust & Kumar 1996).

6.3. *Incorporating Realistic Reconnection Physics (Collisionless Reconnection Condition)*

The physics of reconnection is notoriously complex. However, significant progress has been achieved in recent years and the picture that emerges can be summarized as follows (Uzdensky 2007b). There are two regimes of reconnection: a slow (Sweet–Parker) regime in collisional plasmas and a fast regime in collisionless plasmas. The slow reconnection regime is just as important as the fast one, since, without it, it would be difficult for the system to accumulate significant free magnetic energy before releasing it suddenly *via* fast flare-like events. For practical purposes, the actual rate of fast reconnection is not very critical in our problem, as long as it is faster than the main dynamical time scale (*i.e.*, the orbital period). More important is the fast-reconnection *onset*, or *trigger*, problem, *i.e.*, the question of the transition from the slow to fast reconnection regime occur. The physics of fast collisionless reconnection is very complicated; it involves either two-fluid effects, such as the Hall effect, and/or anomalous

resistivity due to current-driven plasma micro-instabilities. However, despite this complexity, one can formulate a rough criterion for the transition from the slow collisional to the fast collisionless regime (Cassak et al. 2005; Yamada et al. 2006; Uzdensky 2007a,b). We thus plan to utilize this condition to formulate a physically-motivated prescription for handling reconnection. This prescription can then be used directly in our statistical theory or as a sub-grid model in actual MHD simulations of the corona. In our present model in this paper, the reconnection parameter κ, which for simplicity we take to be constant, effectively subsumes all this complexity.

The condition for transition to fast collisionless reconnection involves several physical parameters of the system, including the ambient plasma density. The dependence of the reconnection regime on the density is critical, since it establishes an important feedback that the dynamically subdominant coronal gas exerts on the coronal magnetic field (Uzdensky 2007a,b). In turn, the plasma density in the corona is determined by the disk–corona mass exchange processes, such as evaporation in response to coronal heating, precipitation due to gradual radiative cooling, and magnetocentrifugally and radiatively driven winds. Coupled together, disk–corona mass exchange and the transition to fast collisionless reconnection ensure that the corona is maintained near the state of marginal collisionality and regulate the overall level of coronal activity and its intermittency, as well as the vertical distribution of magnetic energy density and of magnetic dissipation.

These ideas, especially the concept of marginal collisionality, have recently been successfully applied to the solar corona to explain the self-regulating nature of the coronal heating process (Uzdensky 2007a,b) and to the coronae of other main-sequence stars (Cassak et al. 2007). They also have proved very useful for providing a natural explanation for the observed optical depth in the coronae of accreting black holes (Goodman & Uzdensky 2008, in preparation).

Finally, especially for studies of the ADC's interaction with a large-scale disk wind (*e.g.* Brandenburg & von Rekowski 2007), it is important to understand the transition from the force-free regime to the wind regime in which the plasma inertia becomes dynamically important (Uzdensky et al. 2002b). This transition happens near the Alfvén critical surface of the outflow and has a strong effect on magnetic reconnection. In particular, it is expected that, beyond the Alfvén surface, open magnetic field lines will not be able to close back *via* reconnection (*e.g.* Uzdensky 2004).

6.4. *Flux Emergence*

Our model, by construction, is not complete—it needs to be connected to what happens in the disk. In particular, it needs as input a statistical description of the population of small loops, or of their rate of emergence from the disk. This information determines the overall normalization of the loop distribution function and hence the net rates of angular momentum transport and dissipation in the corona. In the models computed here, we have simply assumed a fixed, isotropic distribution of small loops.

The ultimate source of coronal activity is the MHD turbulence in the disk (*e.g.* Galeev et al. 1979; Tout & Pringle 1992; Miller & Stone 2000). Therefore, in order to estimate the rate and form of magnetic flux emergence into the corona, one first needs to understand the properties of MHD turbulence in a stratified disk, with a particular emphasis on the production, evolution, and buoyant rise of magnetic flux tubes (*e.g.* Schramkowski & Achterberg 1993). The best prospect for developing this understanding is through appropriate statistical analyses of MRI turbulence in stratified shearing boxes.

However, the notion of a flux tube in most theoretical discussions (including the present paper) is not sufficiently precise to be applied directly to simulations. What well-defined, measurable, and statistically meaningful quantities correspond to flux tubes or to their rates of emergence? Candidates exist, but it is not clear which is best. Field lines can be found as integral curves of the field and their motions determined, but by what prescription should they be grouped into tubes? Alternatively one might work with Fourier decompositions of the vertical Poynting flux on horizontal planes, or with more general *n*-point correlation functions of the field.

7. SUMMARY AND CONCLUSIONS

In this paper we construct a general theoretical framework for understanding the structure of a strongly-magnetized corona above a turbulent accretion disk. This study is motivated by the need to provide a more solid physical foundation for ADC spectral modeling efforts. It should also act as a connecting bridge between numerical MHD simulations of MRI-turbulent disks and semi-empirical coronal models, and stimulate further theoretical studies of accretion disks coupled to their coronae. We also hope that some of the theoretical tools and ideas developed in this paper will prove useful in solar physics.

One of the major goals of our study is to develop a statistical language appropriate for describing the chaotic coronal magnetic field. Here, we are interested in spatial scales larger than the disk thickness but smaller than its radius and in temporal scales longer than the orbital period but shorter than the overall accretion time. Our approach builds upon the previous work by Tout & Pringle (1996), but uses much more realistic physics in several key aspects and also goes further in analyzing and interpreting the results.

To construct the statistical theory, we represent the corona by an ensemble of elementary magnetic structures, namely, loops connecting two spots on the disk surface (Fig. 1). Each loop is characterized by several primary parameters (*e.g.*, the distance between the footpoints and the orientation). The main object in this study is the *distribution function F* of loops in this parameter space. One of our main goals is to formulate, and then solve, the *loop kinetic equation* (LKE) for this distribution function, similar to the Boltzmann kinetic equation in the statistical theory of gases.

To do this, we first analyze the key physical processes that govern the evolution of individual coronal loops. First, there are several processes that affect the loops individually, such as: (1) emergence of small loops into corona; (2) random footpoint motions due to the disk turbulence; (3) Keplerian shear, stretching loops azimuthally and thereby also making them grow in height. On average, these processes pump energy from the disk into the corona, creating a stressed nonpotential force-free field. In addition, loops may interact with each other *via* episodic reconnection between two individual loops (*c.f.* Tout & Pringle 1996), forming two new loops (see Fig. 5). In our theory reconnection is represented as a binary collision, analogous to binary collisions between atoms in a gas. Correspondingly, we describe loop-loop reconnection by a nonlinear integral operator, similar to Boltzmann's collision operator. In contrast to processes (1)–(3), magnetic reconnection relaxes the accumulated magnetic stresses and

dissipates the accumulated free magnetic energy. Overall, a magnetically-active ADC can be described as a Boiling Magnetic Foam.

Based on these processes we are able to construct the loop kinetic equation. In this equation we characterize the overall rate of reconnection events relative to the Keplerian shear rate by a dimensionless parameter κ. In order to investigate the role of magnetic reconnection in the corona, we solve the loop kinetic equation numerically for several different values of κ. We obtain a *statistical steady state* for each value of κ and find that the steady-state loop distribution function is generally well represented by a orientation-dependent power-law, $F(L,\theta) \sim L^{-\alpha_\kappa(\theta)}$. When Keplerian shear is absent, the distribution function is isotropic, $\alpha_\infty(\theta) = $ const. As the rate of shear relative to reconnection increases (*i.e.*, κ decreases), the distribution becomes more and more anisotropic, with a predominance of toroidal orientation. At the same time, a typical loop grows to a larger size by a stronger shear before its growth is disrupted by reconnection. Thus, the orientation-averaged distribution function becomes shallower as κ is decreased.

Once the distribution function is known, we use it to calculate several important integral quantities related to the energetics of the corona. First, we use a self-consistent *mean-field* approach to compute the magnetic energy density as a function of height, $\bar{B}^2(z)/8\pi$. This quantity represents the collective magnetic pressure of all the neighboring loops that confine any given loop and thus represents another (in addition to reconnection) way in which loops interact with each other in our theory. Although it doesn't enter explicitly into the loop kinetic equation, $\bar{B}(z)$ is very important in our model. In particular, it controls the thickness of loops as a function of height, which affects in turn the cross-section for reconnection. In addition, by requiring that the vertical gradient of the magnetic pressure $\bar{B}^2(z)/8\pi$ be balanced by the magnetic tension within each loop, we self-consistently calculate the equilibrium shape and vertical extent, $Z_{\text{top}}(L)$, of the loops. This, in turn, enables us to calculate some important quantities such as the energy associated with a given loop, the force exerted on its footpoints, etc. We then use these quantities to assess various issues of coronal energetics, including the overall magnetic energy stored in the corona, statistical distribution of coronal energy release events (flares), and the overall angular momentum transferred by the coronal magnetic field. As a result of our parametric study with respect to the reconnection parameter κ, we find that if κ is decreased (*i.e.*, reconnection in the corona is inhibited) beyond a certain value, the slope of the loop distribution function becomes so shallow (namely, shallower than $L^{-3/2}$) that the contribution of large loops to both the magnetic energy and torque starts to dominate, leading to a significant enhancement in these quantities. In our specific model, the critical value of κ is found to be $\kappa_{3/2} \simeq 0.002$.

These results demonstrate that the energetic dominance of coronae is inextricably linked to reconnection processes. They thus motivate further efforts to develop more realistic physical description of reconnection. To reiterate an important point made in the Introduction, the tenuous corona above an accretion disk is likely to be marginally collisionless (Goodman & Uzdensky 2008, in preparation), unlike the dense plasma inside the disk itself. This means that the corona cannot be described by traditional MHD simulations with constant resistivity because of their inability to control or resolve magnetic reconnection, which, as we have shown in this paper, may influence the coronal magnetic energy and angular momentum transfer. Therefore, some kind of a physically-motivated subgrid prescription for reconnection is needed.

REFERENCES

Aly, J. J. 1991, ApJ, 375, L61
—. 1995, ApJ, 439, L63
Beloborodov, A. M. 1999, ApJ, 510, L123
Bisnovatyi-Kogan, G. S. & Blinnikov, S. I. 1976, Soviet Astronomy Letters, 2, 191
Blandford, R. D. & Payne, D. G. 1982, MNRAS, 199, 883
Blandford, R. D. & Znajek, R. L. 1977, MNRAS, 179, 433
Boldyrev, S. & Cattaneo, F. 2004, Physical Review Letters, 92, 144501
Brandenburg, A. & von Rekowski, B. 2007, Memorie della Societa Astronomica Italiana, 78, 374
Browning, P. K. & Priest, E. R. 1984, Sol. Phys., 92, 173
Cassak, P. A., Mullan, D. J., & Shay, M. A. 2007, ArXiv e-prints, 710
Cassak, P. A., Shay, M. A., & Drake, J. F. 2005, Physical Review Letters, 95, 235002
Esin, A. A., McClintock, J. E., & Narayan, R. 1997, ApJ, 489, 865
Fisk, L. A. 2005, ApJ, 626, 563
Fromang, S., Papaloizou, J., Lesur, G., & Heinemann, T. 2007, A&A, 476, 1123
Galeev, A. A., Rosner, R., & Vaiana, G. S. 1979, ApJ, 229, 318
Gammie, C. F. 1999, ApJ, 522, L57
Ghosh, P. & Lamb, F. K. 1978, ApJ, 223, L83
Goldreich, P. & Sridhar, S. 1995, ApJ, 438, 763, (GS95)
Goodman, J. 2003, MNRAS, 339, 937
Heyvaerts, J., Priest, E. R., & Bardou, A. 1996, ApJ, 473, 403
Heyvaerts, J. F. & Priest, E. R. 1989, A&A, 216, 230
Hirose, S., Krolik, J. H., & Stone, J. M. 2006, ApJ, 640, 901
Hughes, D., Paczuski, M., Dendy, R. O., Helander, P., & McClements, K. G. 2003, Physical Review Letters, 90, 131101
Klimchuk, J. A. 2000, Sol. Phys., 193, 53

—. 2006, Sol. Phys., 234, 41
Königl, A. 1991, ApJ, 370, L39
Krolik, J. H. 1999, ApJ, 515, L73
Lesur, G. & Longaretti, P.-Y. 2007, MNRAS, 378, 1471
Liang, E. P. T. & Price, R. H. 1977, ApJ, 218, 247
Livio, M., Ogilvie, G. I., & Pringle, J. E. 1999, ApJ, 512, 100
Lubow, S. H. & Spruit, H. C. 1995, ApJ, 445, 337
Lynden-Bell, D. & Boily, C. 1994, MNRAS, 267, 146
Machida, M., Hayashi, M. R., & Matsumoto, R. 2000, ApJ, 532, L67
Matt, S. & Pudritz, R. E. 2005, ApJ, 632, L135
Merloni, A. & Fabian, A. C. 2001, MNRAS, 321, 549
Miller, J. M., Fabian, A. C., Wijnands, R., Reynolds, C. S., Ehle, M., Freyberg, M. J., van der Klis, M., Lewin, W. H. G., Sanchez-Fernandez, C., & Castro-Tirado, A. J. 2002, ApJ, 570, L69
Miller, J. M., Homan, J., Steeghs, D., Rupen, M., Hunstead, R. W., Wijnands, R., Charles, P. A., & Fabian, A. C. 2006, ApJ, 653, 525
Miller, K. A. & Stone, J. M. 2000, ApJ, 534, 398
Parker, E. N. 1957, J. Geophys. Res., 62, 509
—. 1972, ApJ, 174, 499
—. 1975, ApJ, 201, 494
—. 1983, ApJ, 264, 642
—. 1988, ApJ, 330, 474
Pavlidou, V., Kuijpers, J., Vlahos, L., & Isliker, H. 2001, A&A, 372, 326
Rappazzo, A. F., Velli, M., Einaudi, G., & Dahlburg, R. B. 2007, ArXiv e-prints, 709, apJ, in press
Rees, M. J., Begelman, M. C., Blandford, R. D., & Phinney, E. S. 1982, Nature, 295, 17
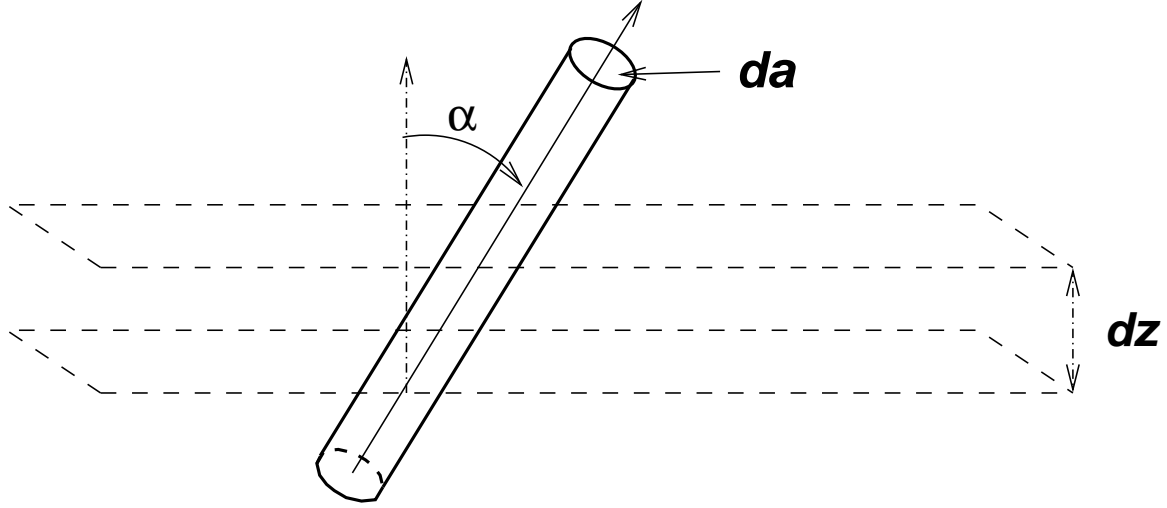Rust, D. M. & Kumar, A. 1996, ApJ, 464, L199

FIG. A15.— A loop segment of area $a(z)$ and angle α, crossing a horizontal slab of thickness dz.

Schekochihin, A. A., Iskakov, A. B., Cowley, S. C., McWilliams, J. C., Proctor, M. R. E., & Yousef, T. A. 2007, New Journal of Physics, 9, 300
Schramkowski, G. P. & Achtergerg, A. 1993, A&A, 280, 313
Shakura, N. I. & Syunyaev, R. A. 1973, A&A, 24, 337
Socrates, A., Davis, S. W., & Blaes, O. 2004, ApJ, 601, 405
Spruit, H. C. & Uzdensky, D. A. 2005, ApJ, 629, 960
Sturrock, P. A. 1991, ApJ, 380, 655
Sturrock, P. A., Antiochos, S. K., & Roumeliotis, G. 1995, ApJ, 443, 804
Sweet, P. A. 1958, in IAU Symposium, Vol. 6, Electromagnetic Phenomena in Cosmical Physics, ed. B. Lehnert, 123
Tout, C. A. & Pringle, J. E. 1992, MNRAS, 259, 604
—. 1996, MNRAS, 281, 219
Turner, N. J., Stone, J. M., & Sano, T. 2002, ApJ, 566, 148
Uzdensky, D. A. 2002, ApJ, 574, 1011

—. 2004, Ap&SS, 292, 573
—. 2007a, Memorie della Societa Astronomica Italiana, 78, 317
—. 2007b, ApJ, 671, 2139
Uzdensky, D. A., Königl, A., & Litwin, C. 2002a, ApJ, 565, 1191
—. 2002b, ApJ, 565, 1205
van Ballegooijen, A. A. 1994, Space Science Reviews, 68, 299
Walsh, R. W. & Ireland, J. 2003, A&A Rev., 12, 1
Weber, E. J. & Davis, L. J. 1967, ApJ, 148, 217
Wilms, J., Reynolds, C. S., Begelman, M. C., Reeves, J., Molendi, S., Staubert, R., & Kendziorra, E. 2001, MNRAS, 328, L27
Yamada, M., Ren, Y., Ji, H., Breslau, J., Gerhardt, S., Kulsrud, R., & Kuritsyn, A. 2006, Physics of Plasmas, 13, 2119

APPENDIX

APPENDIX A: CALCULATION OF $\bar{B}$ IN TERMS OF $\bar{F}(L)$

In this Appendix we calculate the mean magnetic field $\bar{B}(L)$ in terms of the loop distribution function $\bar{F}(L)$ corresponding to a self-consistent atmosphere (see § 3.2).

Consider a horizontal slab of thickness dz at height z (see Fig. A15). Correspondingly, there is a minimal length L of loops that reach above this height. Consider now an arbitrary slender loop $\mathcal{A}$ of length $L' > L$, with a cross-sectional area $a(z)$ and the angle between the loop's direction and the vertical equal to $\alpha(z, L')$. Then the volume that the two segments (ascending and descending) of this loop occupy inside the slab under consideration can be written as

$$dV = 2a(z) \frac{dz}{\cos\alpha(z, L')} . \tag{A1}$$

The volume occupied by all such loops per unit horizontal area of the slab is equal to

$$dV = 2 \int_L^\infty dL' \, a(z) \bar{F}(L') \frac{dz}{\cos\alpha(z, L')} . \tag{A2}$$

Since in our model each loop carries the same amount $\Delta\Psi$ of magnetic flux, the loop cross-sectional area $a(z)$ is the same for all loops at a given height and is simply equal to $\Delta\Psi/\bar{B}(z)$. Thus, the above volume is

$$dV = \frac{2\Delta\Psi}{\bar{B}(z)} \, dz \int_L^\infty \bar{F}(L') \frac{dL'}{\cos\alpha(z, L')} . \tag{A3}$$

But, on the other hand, these loops occupy all the volume within the slab, and so this volume per unit horizontal area ought to be equal to just dz. This gives us the equation that determines $\bar{B}$ as a function of L:

$$\bar{B}(z) = B_0 b(z) = 2\Delta\Psi \int_L^\infty \bar{F}(L') \frac{dL'}{\sqrt{1 - \sin^2\alpha(z, L')}} . \tag{A4}$$

Now, using equation (14), we can replace $\sin\alpha(z,L') = b_{\text{top}}(L')/b(z) = b_{\text{top}}(L')/b_{\text{top}}(L)$ and hence obtain the following integral equation for the function $b(L')$:

$$\int\limits_{L}^{\infty} \frac{\bar{F}(L')\,dL'}{\sqrt{b_{\text{top}}^2(L)-b_{\text{top}}^2(L')}} = \frac{B_0}{2\Delta\Psi} = \text{const}, \tag{A5}$$

which can be rewritten as

$$\int\limits_{0}^{b} \frac{U(b')\,db'}{\sqrt{b^2-b'^2}} = \frac{B_0}{2\Delta\Psi} = \text{const} \tag{A6}$$

where $U(b') \equiv -\bar{F}[L(b')]\,dL/db'$. By substitutions $t = b'^2$, $s = b^2$, and $V(t) = U(b')/2b'$, this equation can be transformed into the Abel integral equation, that can be immediately solved, yielding the following final result:

$$V(s) = \frac{B_0}{2\pi\Delta\Psi\sqrt{s}} \quad \Rightarrow \quad U(b) = -\bar{F}[L(b)]\,dL/db = \frac{B_0}{\pi\Psi_0}. \tag{A7}$$

and hence

$$db = -\frac{\pi\Psi_0}{B_0}\bar{F}(L)\,dL \quad \Rightarrow \quad b(L) = \frac{\pi\Psi_0}{B_0}\int\limits_{L}^{\infty}\bar{F}(L')\,dL', \tag{A8}$$

which is in agreement with our general expectation above.

APPENDIX B: PROOF THAT $\mathcal{E}(L) = 2E_{\text{MAGN}}$

In this Appendix we prove the conjecture that $\mathcal{E}(L) = 2E_{\text{magn}}(L)$. The proof goes as follows.

First, according to equation (31), the force on the loop's footpoint can be expressed in terms of the magnetic field at the top of the loop as

$$f_{\text{fp}}(L) = \frac{\Delta\Psi B_{\text{hor}}(z=0;L)}{4\pi} = \frac{\Delta\Psi B_{\text{top}}(L)}{4\pi}. \tag{B1}$$

Using expression (34) and taking into account that a loop has two legs, we have

$$E_{\text{magn}}(L) = 2\times\frac{\Delta\Psi}{8\pi}\int\limits_{\text{left leg}} B(l)\,dl = \frac{\Delta\Psi}{4\pi}\int\limits_{z=0}^{z_{\text{top}}(L)}\bar{B}(z)\frac{dz}{\cos\alpha} = \frac{\Delta\Psi}{4\pi}\int\limits_{z=0}^{z_{\text{top}}(L)}\frac{\bar{B}^2(z)}{\sqrt{\bar{B}^2-B_{\text{top}}^2}}\,dz. \tag{B2}$$

On the other hand, substituting (B1) into equation (30), we get

$$\mathcal{E}(L) = \frac{\Delta\Psi B_0}{4\pi}\int\limits_{0}^{L} b_{\text{top}}(L')\,dL'. \tag{B3}$$

Integrating this by parts yields

$$\mathcal{E}(L) = \int\limits_{0}^{L} b(L')\,dL' = b(L)L + \int\limits_{b(L)}^{1} L(b')\,db'. \tag{B4}$$

According to (17):

$$\int\limits_{b(L)}^{1} L(b')\,db' = -2\int\limits_{b'=b(L)}^{1} b'\int\limits_{b'}^{1}\frac{[dz(b'')/db'']}{\sqrt{b''^2-b'^2}}\,db''\,db'. \tag{B5}$$

Interchanging the order of integration, we get

$$\int\limits_{b}^{1} L(b')\,db' = -2\int\limits_{b''=b}^{1} db''\,\frac{dz(b'')}{db''}\left(\int\limits_{b'=b}^{1}\frac{b'}{\sqrt{b''^2-b'^2}}\,db'\right)$$

$$= -2\int\limits_{b''=b}^{1}\sqrt{b''^2-b^2}\,\frac{dz(b'')}{db''}\,db''. \tag{B6}$$

On the other hand, according to (17),

$$b(L)L = -2\int\limits_{b''=b(L)}^{1}\frac{b^2\,[dz(b'')/db'']}{\sqrt{b''^2-b^2}}\,db''. \tag{B7}$$

Combining these results we get

$$\mathcal{E}(L) = -2 \int\limits_{b''=b(L)}^{1} \frac{b''^2 \, dz''}{\sqrt{b''^2 - b^2}} = 2 E_{\text{magn}} \, . \tag{B8}$$

End of Proof.